ELSEVIER

Coordination Chemistry Reviews
161 (1997) 81–127

COORDINATION CHEMISTRY REVIEWS

Vibrational coupling effects in the resonance Raman spectra of O_2 adducts of heme proteins and model compounds

Leonard M. Proniewicz [a,b], James R. Kincaid [c,*]

[a] *Chemical Physics Division, Department of Chemistry, Jagiellonian University, R. Ingardena Str. 3, 30-060 Krakow, Poland*
[b] *Regional Laboratory of Physicochemical Analysis and Structural Research, Jagiellonian University, R. Ingardena Str. 3, 30-060 Krakow, Poland*
[c] *Chemistry Department, Marquette University, Milwaukee, WI 53201-1881, USA*

Received 9 August 1996

Contents

* Corresponding author.

PII S0010-8545(97)00001-5

Abbreviations:

$CoAz_{piv}\alpha\alpha$	cobalt(II) 5α,15α-bis[2-(2,2-dimethylpropanamido)phenyl]-10α, 20α-(nonanediamidodi-*o*-phenylene)porphine
$CoAz_{piv}\alpha\alpha$-d_8	β-pyrrole oktadeuteriated $CoAz_{piv}\alpha\alpha$
CoAz2	cobalt(II) 5β,15β:10α,20α-bis(nonanediamidodi-*o*-phenylene)porphyrine
CoAz2-d_8	β-pyrrole oktadeuteriated CoAz2
CoDe2	cobalt(II) 5β,15β:10α,20α-bis(dodecanediamidodi-*o*-phenylene)porphyrine
CoTPP	cobalt(II) tetraphenylporphine
Co(TPP-d_8) or Co(TPP-$^2H_8$)	β-pyrrole oktadeuteriated Co(TPP)
$Co(T_{piv}PP)$	cobalt(II) α^4-"picket fence" porphine
DCP	3,5-dichloropyridine
Hb	hemoglobin
Hb_{Co}	cobalt(II)-substituted hemoglobin
IR	infrared
Im	imidazole
Im-d_2	4,5-dideuterioimidazole
Im-d_3	2,4,5-trideuterioimidazole
Mb	myoglobin
Mb_{Co}	cobalt(II)-substituted myoglobin
py	pyridine
py-$^2H_5$ or py-d_5	perdeuteriated pyridine
RR	resonance Raman
TNOP	tri-*n*-octylphosphine oxide
1-MeIm	1-methylimidazole
1,2-DiMeIm	1,2-dimethylimidazole
4-CNPy	4-cyanopyridine
4-DMAPy	4-(dimethylamino)pyridine
4-MI	4-methylimidazole
4-MI-$^2H_1$ or 4-MI-d_1	N-deuteriated 4-methylimidazole
4-MI-$^2H_2$ or 4-MI-d_2	2,5-dideuterio-4-methylimidazole
α_{Co}	cobalt(II)-substituted hemoglobin α-chain
β_{Co}	cobalt(II)-substituted hemoglobin β-chain
δ	bending vibration
ν	stretching vibration

Keywords: Vibrational coupling effects; Resonance Raman spectroscopy; Dioxygen adducts; Heme proteins

1. Introduction

The mammalian oxygen transport proteins, hemoglobin (Hb) and myoglobin (Mb) are probably the most thoroughly studied of all biomolecules [1–6]. Both are members of the class of proteins, commonly called heme proteins, which contain a heme group (the iron complex of protoporphyrin IX, a tetrapyrrole macrocycle) at the active site. In the case of the oxygen transport proteins (Hb and Mb), the ferrous iron binds molecular oxygen reversibly, oxidation of the iron being inhibited by the protection afforded by the surrounding protein. While the monomeric Mb serves essentially as an oxygen storage protein within muscles, the actual oxygen

transport protein, Hb (which accounts for the bulk of the protein present in red blood cells) is a tetrameric species ($\alpha_2\beta_2$) which exhibits cooperative ligand binding.

Despite the accumulation of a quite extensive body of knowledge, questions remain unanswered, even at an essentially fundamental level. For example, both proteins possess a (distal) histidylimidazole positioned so as to facilitate hydrogen bonding with the bound dioxygen. The importance of such H-bonding for the oxygenation process continues to attract much attention [7–13]. Perhaps even more surprising is the fact that dispute still continues concerning the number of stable structures [14–19].

The intense interest in the details of dioxygen binding to these proteins prompted an extensive effort by many research groups to develop and study model compounds in an attempt to understand the steric and electronic factors which control oxygen binding in the native systems. These elaborately designed model systems include the "picket-fence" [20–24], "capped" [25–29], "strapped" [30–35], and "jellyfish" [36–40] metalloporphyrins, among others. The essential rationale behind the use of such systems is, of course, that structural and environmental perturbations can be well-controlled and related to observed spectroscopic and functional response. Thus, in order to most effectively employ such model systems, it is important to establish reliable spectroscopic probes of the key elements (i.e., the $Fe–O_2$ fragment) in the models and native systems.

Traditionally, vibrational spectroscopy (both infrared (IR) and Raman) has served as a powerful probe of ligand binding to metal centers in coordination and organometallic compounds [41]. Thus, it is not surprising that much effort has been expended in attempts to apply these techniques to the study of ligand binding to heme proteins and model compounds [42–45]. In principle, these methods offer great potential for detection of slight changes in bonding associated with subtle structural perturbations inasmuch as, theoretically, they may provide a direct probe of the bound O_2 through detection of the fundamental vibrations of the $Fe–O_2$ fragment (i.e., ν(O–O), ν(Fe–O) and δ(FeOO)). Unfortunately, despite this inherent potential, vibrational spectroscopic studies of these issues and these systems have been hampered by ambiguities arising from several technical and interpretational difficulties.

In the case of IR spectroscopy, the inherently weak ν(O–O) absorption is obscured by an envelope of features associated with vibrations of the peptide. While it is possible, in principle, to extract the weak ν(O–O) absorptions from the other bands in this congested spectral region by employing difference techniques, as discussed in detail by Caughey and co-workers in their report of carefully conducted IR studies [17], many factors can give rise to artifacts in these difference spectra. Thus, there is some impetus to explore the utility of Raman spectroscopy for the study of these issues.

While the normal Raman effect is notoriously weak and lacks the sensitivity to study dilute solutions, the resonance Raman (RR) effect is ideally suited to the study of heme proteins. In this technique great increases in sensitivity and selectivity are realized by using (laser) excitation wavelengths in resonance with the strong electronic absorption bands associated with the active site chromophore (i.e., the

oxygenated heme group). Since the first RR spectra of heme proteins was reported by Strekas and Spiro [46], the technique has been applied by many workers to investigate heme structure in a large number of derivatives [47–53]. Unfortunately, it has not been possible to identify conditions under which the ν(O–O) of the O_2 adducts of native Hb and Mb is effectively enhanced, thus eliminating the possibility of directly probing the Fe–O_2 fragment by observation of this mode.

A major breakthrough was achieved by Yu and co-workers [15,16,54] who demonstrated that the ν(O–O) of the corresponding cobaltous analogues is strongly enhanced by excitation near the very intense (so-called Soret) band which occurs near 400 nm, though it should be pointed out that the mechanism of enhancement is thought to be associated with an underlying charge-transfer transition ascribable to the Co–O_2 fragment. The fact that these cobalt-substituted analogues retain the gross structural and functional properties of the native system [55–59] validates the utility of RR studies of these as an effective strategy to probe the factors which influence oxygen binding.

Given the availability of an effective probe (i.e., RR spectroscopy of the cobalt analogues), systematic studies employing model compounds were undertaken by our group in order to gain insight into the steric, electronic and environmental factors which influence the vibrational spectral patterns of the model compounds so as to provide an interpretive framework for analysis of the RR spectra of the cobalt-substituted proteins.

The purpose of the present review is to summarize the results of these and related studies. As will be apparent, while the essential assumption that RR studies of model compounds are useful for the interpretation of the spectra of these proteins is demonstrated, it will also be clear that the spectra of both the proteins and model systems are severely complicated by an unusually strong (coupling) interaction between the ν(O–O) and internal modes of other fragments of the system, including the trans-axial base and intimately associated molecules of the environment.

2. Vibrationally coupled dioxygen in model compound systems

2.1. Coupling with internal modes of the trans-axial base

2.1.1. Spectral consequences of the effect

2.1.1.1. O_2 adducts of pyridine complexes: the first evidence of the effect. It is appropriate to begin with a quite simple chemical system; that of the dioxygen adduct of the pyridine complex of cobalt tetraphenylporphine, O_2CoTPP(py) [60–62]. Actually, in most of our studies we utilize the β-pyrrole deuteriated analogues of the various porphyrins in order to avoid an annoying overlap of the $\nu(^{18}O–^{18}O)$ with a strong macrocycle mode which occurs near 1084 cm^{-1} in the case of the natural abundance porphyrins. Thus, for studies with TPP we utilize TPP-$^2H_8$ (abbreviated also as TPP-d_8), so the first example to be considered is O_2Co(TPP-$^2H_8$)(pyr), whose RR spectra are shown in Fig. 1. Traces A and B give

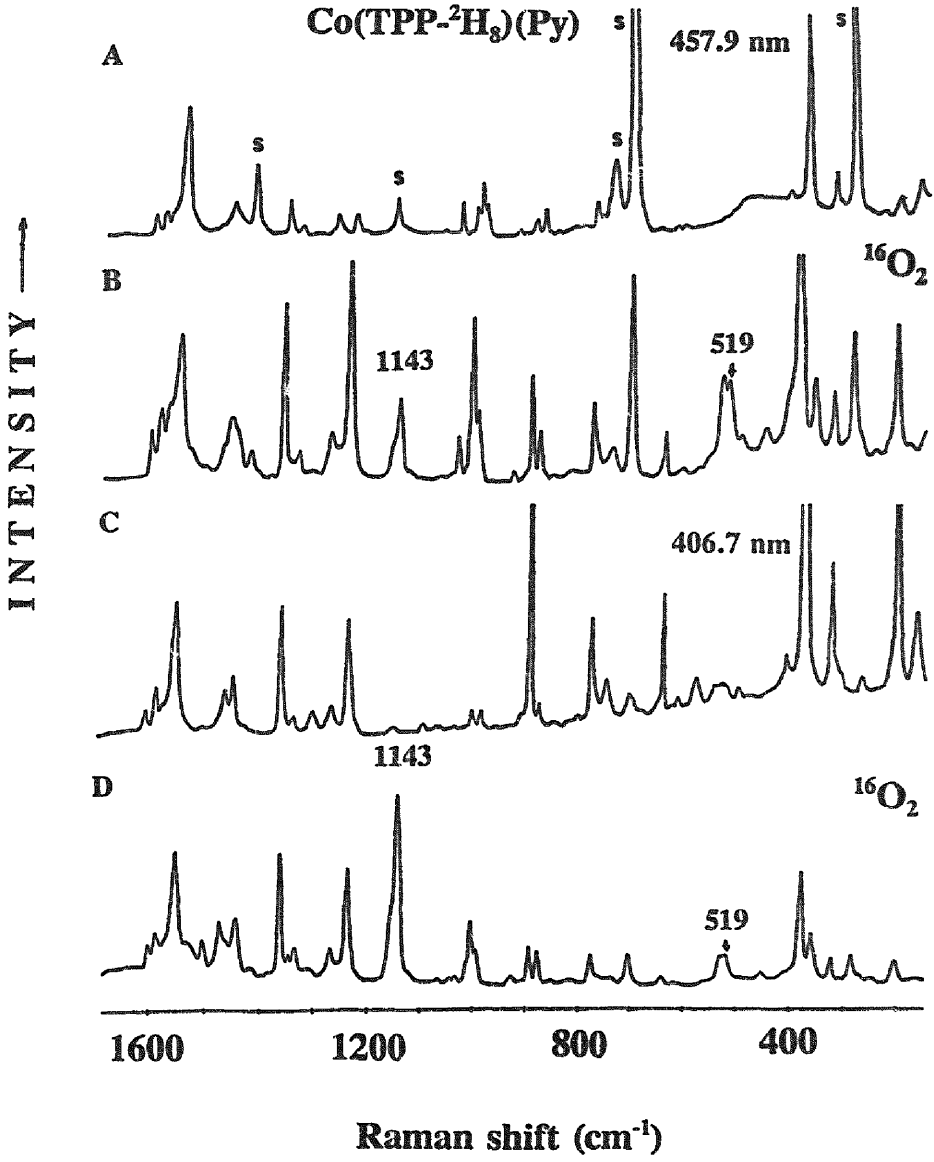

Fig. 1. Resonance Raman spectra of Co(TPP–$^2H_8$) in CH_2Cl_2 solution containing 3% pyridine at −90°C: (A) Co(TPP–$^2H_8$)+no oxygen, 457.9-nm excitation; (B) Co(TPP–$^2H_8$)+$^{16}O_2$ (ca. 4 atm.), 457.9-nm excitation; (C) Co(TPP–$^2H_8$)+no oxygen, 406.7-nm excitation; (D) Co(TPP–$^2H_8$)+$^{16}O_2$ (ca. 4 atm.), 406.7-nm excitation. "S" denotes the solvent bands (adapted from Ref. [60]).

the RR spectra of Co(TPP-$^2H_8$)(pyr) and the corresponding O_2 adduct [O_2Co(TPP-$^2H_8$)(pyr)], respectively, obtained with 457.9 nm excitation. The strong new feature at 1143 cm^{-1} appearing upon oxygenation is associated with the $\nu(^{16}O–^{16}O)$ mode (vidè infra). The spectra shown in traces C and D were obtained using 406.7 nm excitation, where it is evident that the ν(O–O) band is more strongly enhanced relative to the porphyrin macrocycle and solvent bands. For this reason, the 406.7 nm line is used almost exclusively to obtain the RR spectra of the O_2 adducts discussed here.

The region wherein the ν(O–O) is expected to occur is shown in expanded scale in Fig. 2, which illustrates the spectra obtained for variously isotopically labeled derivatives. The solid line in trace A gives the spectrum for the $^{16}O_2$ adduct obtained in CH_2Cl_2. In fact, there it is seen that the strong 1143 cm^{-1} feature possesses a high frequency shoulder which is associated with a solvent mode (the 1156 cm^{-1} feature). For this reason, the spectrum was also obtained in $C^2H_2Cl_2$ (abbreviated also as CD_2Cl_2) in order to eliminate this spectral overlap. As will be discussed later, this near coincidence of the $\nu(^{16}O–^{16}O)$ with the solvent mode gives rise to a quite interesting effect, but for now it is useful to avoid this complication by considering only the spectrum obtained in $C^2H_2Cl_2$, shown by the dashed line in trace A. Thus, in $C^2H_2Cl_2$, the $\nu(^{16}O–^{16}O)$ is observed as a strong symmetric band located at 1148 cm^{-1}.

In many, if not most, metal (M) complexes of diatomic ligands (XY) (i.e., M(XY)), the XY fragment behaves approximately as a simple harmonic oscillator. Thus, given the value of 1148 cm^{-1} for the inherent frequency of the $\nu(^{16}O–^{16}O)$, it is expected that the $\nu(^{18}O–^{18}O)$ would occur at 1082 cm^{-1} (i.e., the isotopic shift, $\Delta\nu^{16}O/^{18}O$, is expected to be 66 cm^{-1}). However, as can be seen from inspection of trace B (solid line), *two* new features appear when $^{16}O_2$ is replaced by $^{18}O_2$. The strong band is located at 1084 cm^{-1}, while the weaker, lower frequency, feature occurs at 1067 cm^{-1}. This 1067 cm^{-1} ("satellite") feature has a frequency which is similar to that of an internal mode of pyridine [63–65] and it was suspected that it may be ascribable to the axial ligand.

As the spectrum shown by the dashed line in trace B confirms, this satellite band disappears where pyridine-$^2H_5$ is used in place of pyridine, confirming that the 1067 cm^{-1} arises from the pyridine in the sample. However, it is important to note several key points. First, when the pyridine is replaced by pyr-$^2H_5$, not only does the 1067 cm^{-1} feature disappear, but the strong 1084 cm^{-1} mode shifts down by 2 cm^{-1} to 1082 cm^{-1}. Furthermore, it is important to note that in the case of $^{16}O_2$ adduct (trace A), this 1067 cm^{-1} feature is not significantly enhanced. Finally, it is important to point out that the relative concentrations of pyridine in both cases ($^{16}O_2$ and $^{18}O_2$) are approximately the same, and thus both spectra are relatively

Fig. 2. Resonance Raman spectra (406.7-nm excitation) of O_2 adducts of Co(TPP-$^2H_8$) in CH_2Cl_2 solution containing 3% pyridine at −90°C under ca. 4 atm. of O_2 pressure: (A) $^{16}O_2$, dotted line shows the position of $\nu(^{16}O–^{16}O)$ in $C^2H_2Cl_2$ at 1148 cm^{-1}; (B) $^{18}O_2$, dotted line shows the fragment of the spectrum when pyridine-$^2H_5$ has been used as a base instead of neat pyridine ($\nu(^{18}O–^{18}O)$ at 1082 cm^{-1} with pyridine-$^2H_5$); (C) "scrambled" O_2:$^{16}O_2+2^{16}O^{18}O+^{18}O_2$ (adapted from Ref. [60]).

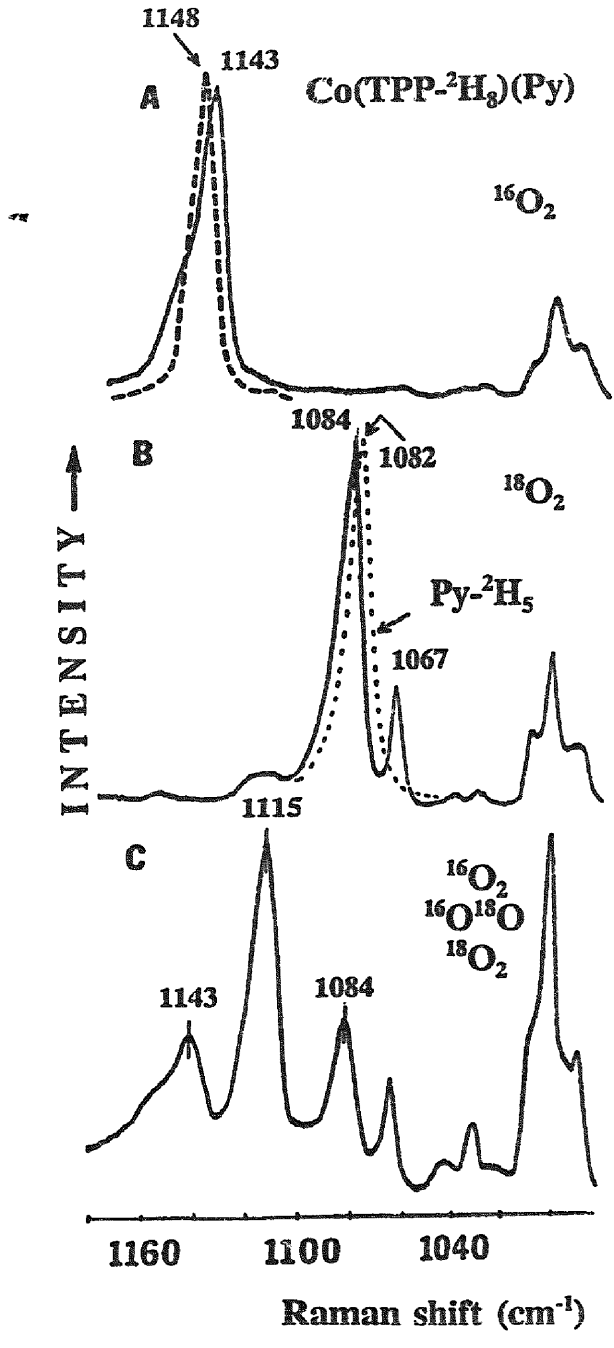
1148
1143
A
Co(TPP-$^2H_8$)(Py)
$^{16}O_2$
1084
1082
B
$^{18}O_2$
Py-$^2H_5$
1067
INTENSITY
1115
C
$^{16}O_2$
$^{16}O^{18}O$
$^{18}O_2$
1143
1084
1160
1100
1040
Raman shift (cm^{-1})

independent of pyridine concentration (up to much higher concentrations). Essentially the same results are obtained for complexes in which molecular ratio of Co(TPP-$^2H_8$) to pyridine is 1:1; i.e., when there is no excess pyridine in solution [61,62].

The spectrum shown in trace C corresponds to that obtained for a sample of so-called "scrambled oxygen", which contains a mixture of $^{16}O_2$, $^{16}O^{18}O$, and $^{18}O_2$. This mixture is obtained by subjecting (1:1) mixtures of $^{16}O_2$ and $^{18}O_2$ to an electrical discharge from a Tesla coil [66]. Prolonged exposure to the discharge yields the statistical distribution of $^{16}O_2$:$^{16}O^{18}O$:$^{18}O_2$ (1:2:1), but abbreviated treatment can produce lower amounts of the $^{16}O^{18}O$ component. The relative concentrations can be conveniently monitored by Raman spectroscopy of the gas in the bulb and the discharge halted when the desired ratio is reached. In most cases the statistical ratio was employed, although in special situations (vidè infra) it is quite useful to employ both (1:2:1) and (1:1:1) mixtures. As can be seen in trace C, in addition to the 1143 cm^{-1} envelope and the 1084/1067 cm^{-1} doublet (which are associated with the $^{16}O_2$ and $^{18}O_2$ present in the sample), a strong symmetric feature is observed at 1115 cm^{-1} which can be ascribed to $\nu(^{16}O^{18}O)$.

Careful consideration of the spectra shown in Fig. 2 reveals the following points. In the absence of labeling experiments (i.e., considering only the spectra shown with solid lines), it would appear that the ν(O–O) occurs at 1143 cm^{-1} in the case of $^{16}O_2$ and shifts to 1084 cm^{-1} upon $^{18}O_2$ substitution and that a mysterious "satellite" band occurs at 1067 cm^{-1} for the $^{18}O_2$ adduct. Using these frequencies, non-ideal isotopic shifts are derived. Thus, the observed $\Delta\nu(^{16}O_2/^{18}O_2)$ = 1143–1084 = 59 cm^{-1} and $\Delta\nu(^{16}O_2/^{16}O^{18}O)$ = 1143–1115 = 28 cm^{-1}, while the observed $\Delta\nu(^{16}O^{18}O/^{18}O_2))$ = 1115–1084 = 31 cm^{-1}. However, upon elimination of the "interfering" modes associated with other fragments of the system (i.e., the spectra shown by dashed lines), the observed isotopic shifts are in perfect agreement with expectation. Thus, $\Delta\nu(^{16}O_2/^{16}O^{18}O)$ = 1148–1115 = 33 cm^{-1}, $\Delta\nu(^{16}O^{18}O/^{18}O_2)$ = 1115–1082 = 33 cm^{-1} and, of course, $\Delta\nu(^{16}O_2/^{18}O_2)$ = 1148–1082 = 66 cm^{-1}.

2.1.1.2. Implications for structural interpretations of spectra. The fact that such effects assume more importance than as interesting spectroscopic phenomena is perhaps best illustrated by consideration of the spectra obtained for the $^{16}O_2$ adducts of the complexes of cobalt porphyrins with 1,2-dimethylimidazole, 1,2-DiMeIm, whose spectra are shown in Figs. 3(A) and 4(A). In both cases, two relatively strong bands appear in the region near 1140–1160 cm^{-1}. In fact, in the first known report of the RR spectra of an O_2 adduct of a cobalt substituted model compound [16], the appearance of two bands for the $^{16}O_2$ was unfortunately taken as evidence for the presence of two distinct conformers. However, as evident upon inspection of the spectra of the $^{18}O_2$ analogues (Figs. 3(B) and 4(B)), only a single strong band is observed for $\nu(^{18}O–^{18}O)$. It should be pointed out that, in the case of $^{18}O_2$Co(T_{piv}PP)(1,2-DiMeIm) (Fig. 4(B)), the weak low frequency shoulder on the $\nu(^{18}O–^{18}O)$ band is due to overlap with an internal mode of the porphyrin at 1078 cm^{-1}; i.e., in this case the deuteriated porphyrin was not employed. Clearly,

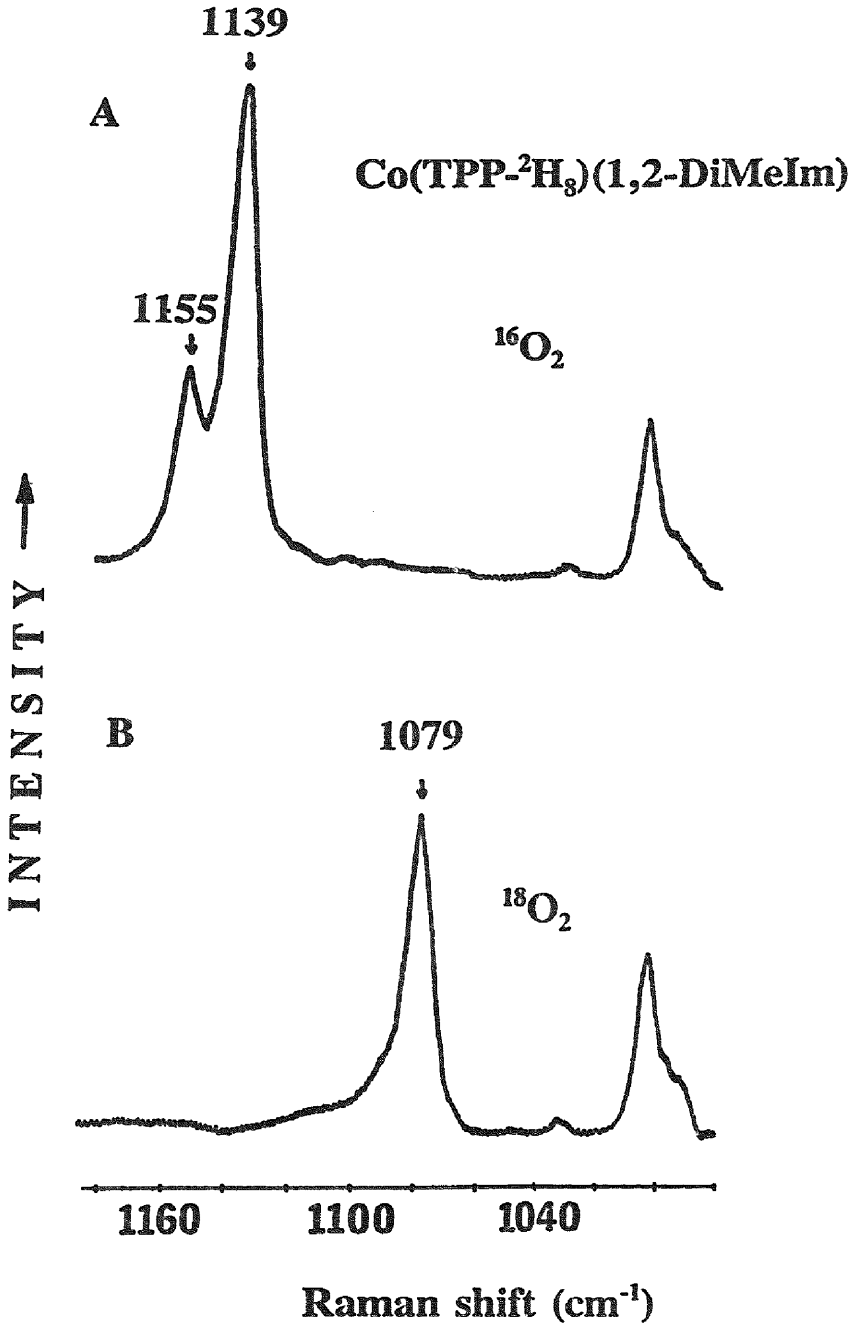

Fig. 3. Resonance Raman spectra (406.7-nm excitation) of dioxygen adducts of Co(TPP-$^2H_8$) in CH_2Cl_2 containing 3% of 1,2-dimethylimidazole at −90°C under ca. 4 atm. of O_2 pressure: (A) $^{16}O_2$; (B) $^{18}O_2$ (adapted from Ref. [60]).

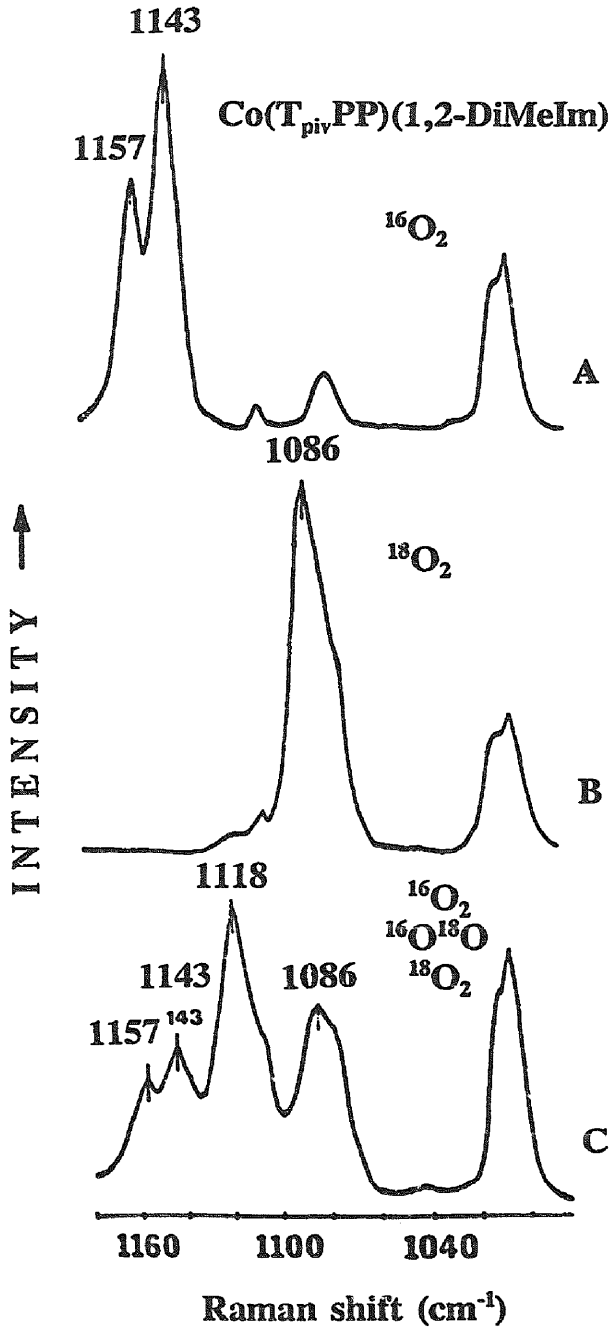

Fig. 4. Resonance Raman spectra (406.7-nm excitation) of dioxygen adducts of Co(T_{piv}PP) in CH_2Cl_2 containing 3% of 1,2-dimethylimidazole at −90°C under ca. 4 atm. of O_2 pressure: (A) $^{16}O_2$; (B) $^{18}O_2$; (C) $^{16}O_2/^{16}O^{18}O/^{18}O_2 = 1/2/1$ (adapted from Ref. [60]).

the doublet structure observed in the case of $^{16}O_2$ cannot be attributed to two different chemical forms.

Considering the case of Co(TPP-$^2H_8$) (Fig. 3), given the value of 1079 cm^{-1} for the inherent frequency of $\nu(^{18}O–^{18}O)$, it is expected that the inherent value of $\nu(^{16}O–^{16}O)$ is 1145 cm^{-1} (i.e., 1079 + 66 cm^{-1}). The base 1,2-DiMeIm is known to have an internal mode located near 1150 cm^{-1} [60]. Thus, interaction of the $\nu(^{16}O–^{16}O)$ with this base mode induces a low frequency shift of the "ν(O–O)" mode (by 5–6 cm^{-1}) to 1139 cm^{-1} and a corresponding shift to high frequency for the "base" mode by 5–6 cm^{-1} (i.e., 1150–1155 cm^{-1}). The point to be emphasized is that, if care is not taken to perform required isotopic labelling studies, erroneous structural interpretations can arise. Therefore, it became important to perform extensive and systematic studies on many complexes in order to assess the magnitude and clarify the details of this type of coupling interaction involving coordinated O_2.

2.1.1.3. Systematic model compound studies

2.1.1.3.1. 4-Methylimidazole. An example where each of the O_2 isotopomers can couple with a single internal mode of the trans-axial ligand (and one that is of interest from the standpoint of having direct relevance to the heme protein spectra) is the case of O_2 adducts of cobalt porphyrin complexes with 4-methylimidazole (4-MI), a close structural analoge of the proximal histidylimidazole of the proteins [67]. The normal Raman spectra of 4-MI, its N-deuteriated (4-MI-$^2H_1$) and ring deuteriated (4-MI-$^2H_2$) analoges are given in Fig. 5. There it is seen that the natural abundance 4MI possesses a band at 1107 cm^{-1}, whereas 4-MI-$^2H_2$ (abbreviated also as 4-MI-d_2) exhibits no bands in the region between 1100 and 1160 cm^{-1}.

The spectra of the O_2 adducts of Co(TPP-d_8)(4-MI) and Co(TPP-d_8)(4-MI-d_2) are given in Fig. 6. In the case of the $^{16}O_2$ adduct in the presence of 4-MI (Fig. 6(A), solid line), the ν(O–O) mode is observed at 1146 cm^{-1} along with a weak feature at 1105 cm^{-1}. When 4-MI-d_2 replaces 4-MI (trace A, dotted line), the 1105 cm^{-1} band disappears. Simultaneously, the $\nu(^{16}O–^{16}O)$ downshifts by 3 cm^{-1}. The $\nu(^{18}O–^{18}O)$ mode of $^{18}O_2$Co(TPP-d_8)(4-MI) is observed at 1077 cm^{-1} as a strong feature accompanied by the weak band at 1111 cm^{-1} (trace B, solid line). Again, as in the case of $^{16}O_2$ dioxygen adduct, this weak band disappears (and $\nu(^{18}O–^{18}O)$ upshifts by 3 cm^{-1}) when 4-MI-d_2 is used. This spectral behavior is consistent with that expected for vibrationally coupled dioxygen. The $\nu(^{16}O–^{16}O)$, having an inherent frequency of 1143 cm^{-1}, interacts with the 1107 cm^{-1} 4-MI mode (Fig. 6(A)) giving rise to two bands at 1146 and 1105 cm^{-1}, respectively; i.e., the higher frequency band upshifts, while the lower frequency band downshifts by the same amount (2–3 cm^{-1}). Upon substituting 4-MI-d_2, this coupling is eliminated. The 1105 cm^{-1} band disappears revealing the inherent frequency of $\nu(^{16}O–^{16}O)$ as 1143 cm^{-1}. The same explanation holds for the $^{18}O_2$ adduct.

These somewhat subtle effects of vibrationally coupled dioxygen are a consequence of rather weak coupling between modes which are relatively far separated (ca. 30–35 cm^{-1}). Fig. 6(C) provides a dramatic illustration of the remarkable spectro-

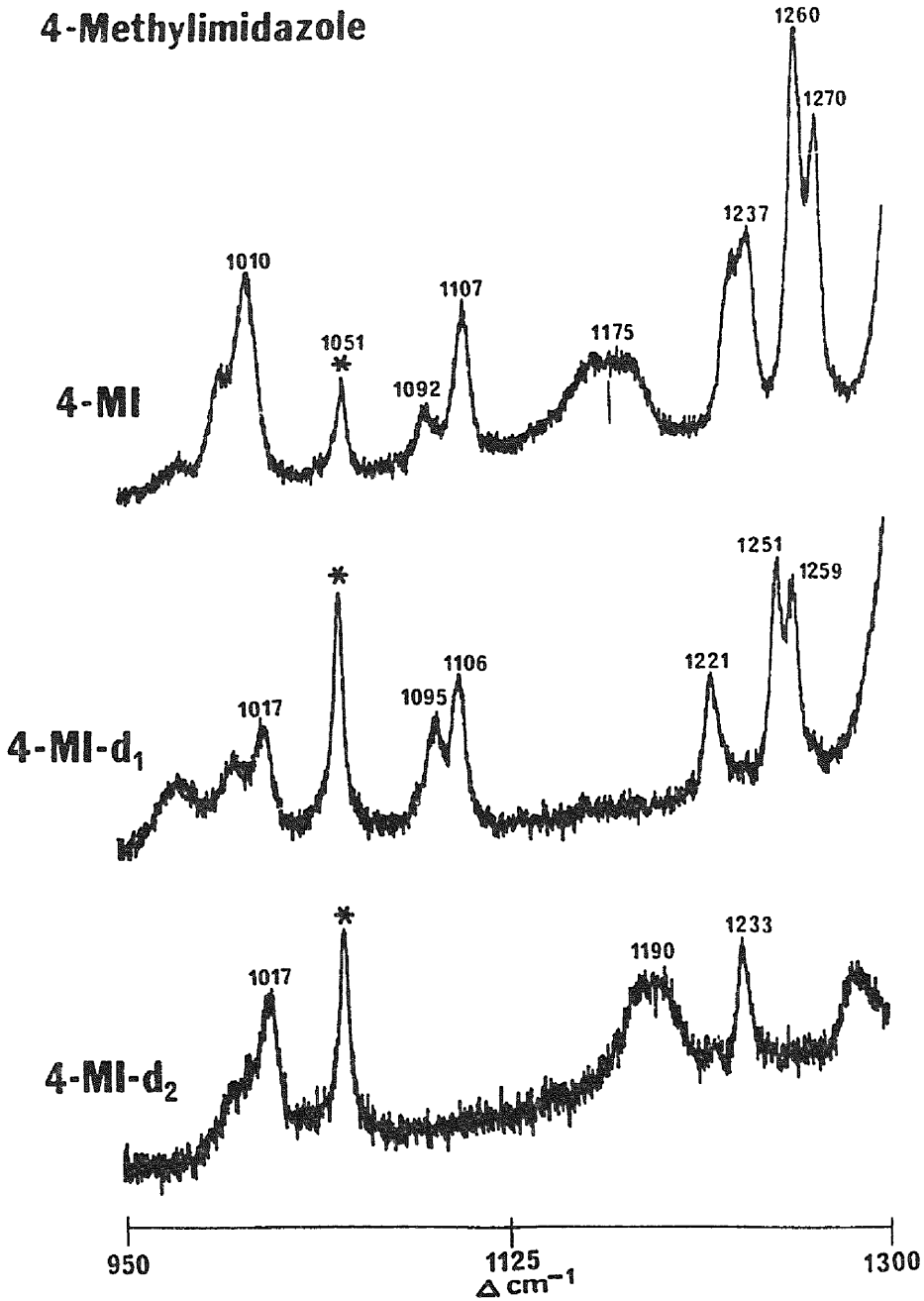

Fig. 5. Raman spectra of 4-methylimidazole and deuteriated analogues (see text) in $C^2H_2Cl_2$ measured at room temperature with excitation at 406.7 nm (10 mW of laser power at the sample). Asterisks mark solvent bands (from Ref. [67]).

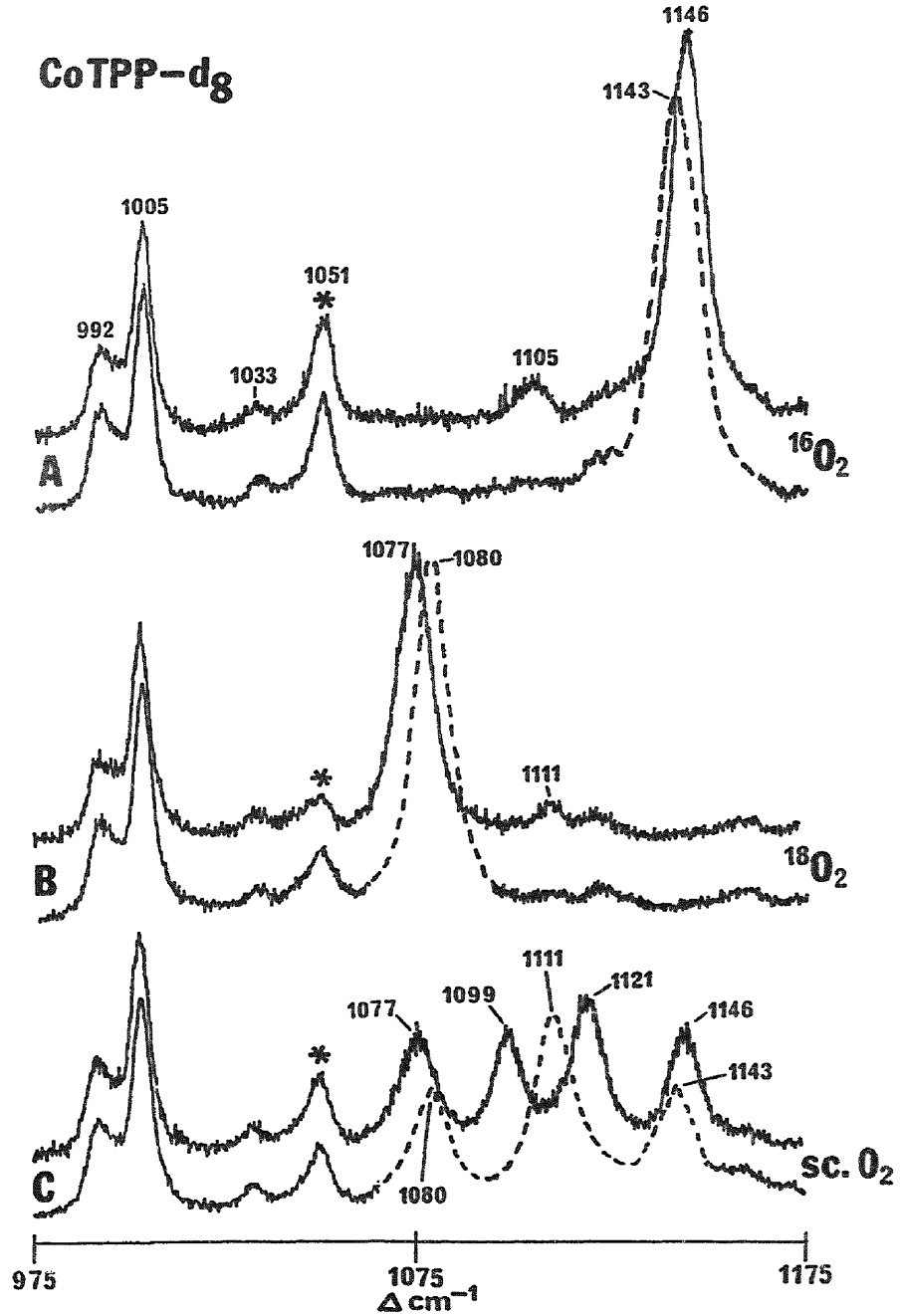

Fig. 6. Resonance Raman spectra of dioxygen adducts of Co(TPP-$^2H_8$) in the presence of 4-MI (solid line) or 4-MI-$^2H_2$ (dashed line) at −90°C in $C^2H_2Cl_2$ with excitation at 406.7 nm (10 mW of laser power at the sample): (A) $^{16}O_2$; (B) $^{18}O_2$; (C) $^{16}O_2$ $^{16}O^{18}O/^{18}O_2$ (1/2/1). Asterisks mark solvent bands (from Ref. [67]).

scopic manifestation of strong vibrational coupling; i.e., as the interacting modes become frequency matched. Given inherent $\nu(^{16}O–^{16}O)$ and $\nu(^{18}O–^{18}O)$ frequencies of 1143 and 1080 cm^{-1}, $\nu(^{16}O–^{18}O)$ is predicted to occur at ~1111 cm^{-1}, i.e., midway between 1143 and 1080 cm^{-1}. Accordingly, in the case of 4-MI-d_2 (no base mode is present in this region), the $\nu(^{16}O–^{18}O)$ is observed at 1111 cm^{-1} along with $\nu(^{16}O–^{16}O)$ and $\nu(^{18}O–^{18}O)$ at 1143 and 1080 cm^{-1}, respectively. When 4-MI is used (trace C, solid line), the RR spectrum changes dramatically. The close matching of $\nu(^{16}O–^{18}O)$, having an inherent frequency of 1111 cm^{-1}, with the interacting 4-MI mode at ~1107 cm^{-1} results in very efficient coupling which gives rise to two fairly strong bands, of roughly equal intensity, located at ±8–10 cm^{-1} from their inherent frequencies of ~1107 and 1111 cm^{-1} (i.e., at 1099 and 1121 cm^{-1}).

2.1.1.3.2. 3,5-Dichloropyridine. Having documented the existence of this coupling effect in several different model systems, a system was sought which would prove useful for a thorough and systematic study. In the case of O_2 adducts of cobalt porphyrin complexes with 3,5-dichloropyridine (DCP), the vibrational interaction between ν(O–O) and an internal mode of DCP is of adequate strength to permit an investigation of the energy-matching dependence of the interaction modes over a controlled range of frequency separations [68–71].

The spectra of the O_2 adducts of Co(TPP-d_8)(DCP) in $C^2H_2Cl_2$ are shown in Fig. 7. As is seen in trace A, in the spectrum of the $^{16}O_2$ adduct, a strong band is observed at 1160 cm^{-1} along with a weak feature at 1112 cm^{-1}. In the case of the $^{13}O_2$ adduct (trace B) both the 1160 and 1112 cm^{-1} bands disappear and are replaced by bands occurring at 1121 cm^{-1} (weaker) and 1086 cm^{-1} (stronger). One possible interpretation of these observations is that the dioxygen adduct exists in two chemical (or structural) forms which exhibit $\nu(^{16}O–^{16}O)$ frequencies at 1160 and 1112 cm^{-1}. The corresponding $^{18}O_2$ adducts would also be expected to exhibit two $\nu(^{18}O–^{18}O)$ bands, and two bands are indeed observed at 1121 and 1086 cm^{-1}. According to this interpretation, the form exhibiting the highest frequency ν(O–O) would yield a $\Delta\nu(^{16}O_2–^{18}O_2)$ of 39 cm^{-1} (1160–1121 cm^{-1}) and the second form (lower frequency ν(O–O)) would yield a $\Delta\nu(^{16}O_2–^{18}O_2)$ of only 26 cm^{-1} (1112–1086 cm^{-1}). These $\Delta\nu(^{16}O_2–^{18}O_2)$ values are quite small compared to that predicted (~65 cm^{-1}) by the diatomic harmonic oscillator approximation. Furthermore, given the observed intensities of these bands, this approach would also require that either the relative population or the inherent RR scattering efficiencies of the two isotopic species are different. That is, it would be necessary to consider the higher frequency form to predominate for the $^{16}O_2$ adduct and the lower frequency form to be the major form for the $^{18}O_2$ adduct. Alternatively, it would require that $\nu(^{16}O–^{16}O)$ has an inherently greater scattering efficiency in the second chemical form.

Such tenuous arguments can be avoided by invoking vibrational coupling of

Fig. 7. Resonance Raman spectra of Co(TPP-d_8)(DCP)O_2 in $C^2H_2Cl_2$ at −90°C (excitation at 406.7 nm, 10 mW laser power at the sample): (A) $^{16}O_2$; (B) $^{18}O_2$; (C) $^{16}O_2$: $^{16}O^{18}O$:$^{18}O_2$ (1:2:1); (D) $^{16}O_2$:$^{16}O^{18}O$:$^{18}O_2$ (1:1:1). The 1050 cm^{-1} is a solvent band (from Ref. [68]).

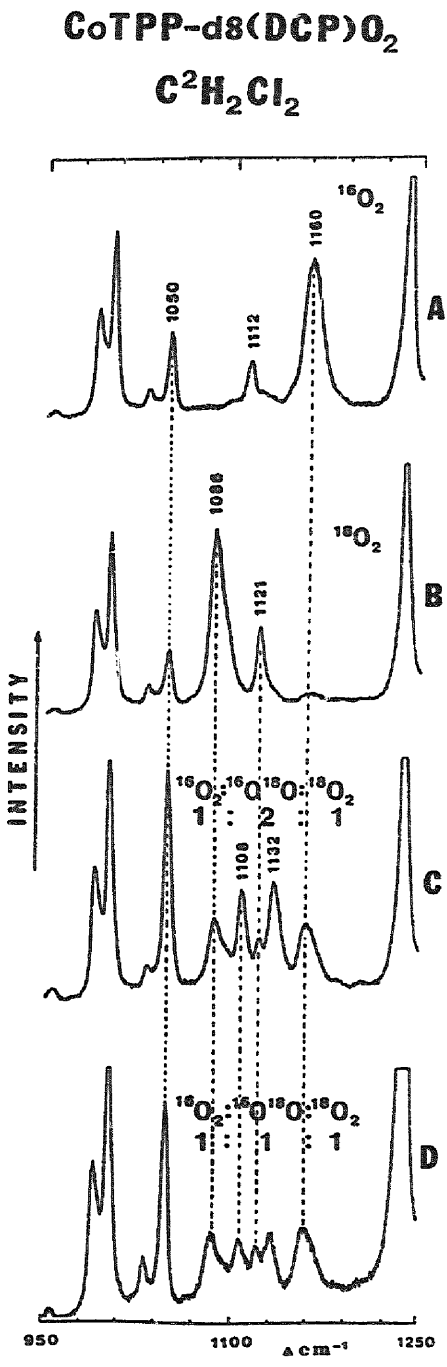
CoTPP-d8(DCP)O2
C2H2Cl2
16O2
1160
1050
1112
A
1086
18O2
1121
B
INTENSITY
16O2 16O18O 18O2
1 2 1
1108
1132
C
16O2 16O18O 18O2
1 1 1
D
950
1100
Δcm-1
1250

ν(O–O) with an internal mode of the (trans) coordinated DCP. The Raman spectrum of free DCP in CH_2Cl_2 exhibits, among others, two strong bands of comparable intensity at 1109 and 1012 cm^{-1}. While small shifts may be associated with coordination of the DCP, it is reasonable to expect internal modes of the coordinated ligand to occur near these 1110 and 1010 cm^{-1} regions. Inasmuch as the inherent frequencies of the ν(O–O) modes for the various dioxygen isotopomers apparently occur between $\sim$1090 and $\sim$1160 cm^{-1}, interactions with the $\sim$1110 cm^{-1} ligand mode may be anticipated. As will be discussed later, such interactions may be treated quantitatively to provide estimates of induced shifts and relative intensities of the coupled modes [71]. However, the interpretation of the spectral data for this system (shown in Fig. 7) can be briefly summarized here, as follows. The strong 1160 cm^{-1} feature (trace A) is assigned to $\nu(^{16}O–^{16}O)$ and the weaker 1112 cm^{-1} feature to an enhanced (coupled) internal mode of the coordinated DCP. Their inherent frequencies are 1156 and 1115 cm^{-1}, respectively; i.e., the higher frequency component is upshifted, while the lower frequency component is downshifted (by the same amount, 3–4 cm^{-1}) because of the vibrational coupling interaction. Given an inherent frequency for the $\nu(^{16}O–^{16}O)$ mode of 1156 cm^{-1}, the harmonic approximation predicts the occurrence of $\nu(^{18}O–^{18}O)$ at 1090 cm^{-1}. This latter frequency is also close in energy to the internal ligand mode at 1115 cm^{-1}. Interaction of these two modes yields two RR bands, both of which are shifted from their inherent frequencies by 5 ± 1 cm^{-1} (the accuracy of the frequency measurement is ± 1 cm^{-1}); i.e., bands are observed at 1086 and 1121 cm^{-1} (trace B).

Further confirmation of this coupling, and a clear demonstration of the spectroscopic complexity that may result from such behavior, are provided by the study of adducts formed with scrambled dioxygen (i.e., $^{16}O_2$:$^{16}O^{18}O$:$^{18}O_2$). The RR spectrum of the solution containing the adduct formed in the presence of 1:2:1 scrambled dioxygen is shown in Fig. 7(C). In this figure, the band observed at 1160 cm^{-1} is readily assignable to the $^{16}O_2$ adduct, while the 1121 and 1086 cm^{-1} features are attributable to the $^{18}O_2$ adduct. However, new features are observed at 1132 and 1108 cm^{-1}. The 1108 cm^{-1} band overlaps and obscures the band expected at 1112 cm^{-1} (i.e., the weak ligand mode associated with the $^{16}O_2$ adduct). This complex spectroscopic pattern is entirely consistent with the above interpretation. Thus, given a $\nu(^{16}O–^{16}O)$ inherent frequency of 1156 cm^{-1}, the diatomic harmonic approximation would yield a $\nu(^{16}O–^{18}O)$ frequency of 1123 cm^{-1}. This frequency is within 8 cm^{-1} of the inherent frequency of the coordinated ligand mode, and these two vibrationally couple, resulting in splitting of the coupled modes. Namely, interaction of the (high frequency) $\nu(^{16}O–^{18}O)$ with the 1115 cm^{-1} DCP mode results in shifts of the coupled modes by $+9$ cm^{-1} (1123–1132 cm^{-1}) and -7 cm^{-1} (1115–1108 cm^{-1}) from their inherent frequencies. Further support for this explanation is provided by the spectrum of the 1:1:1 scrambled dioxygen adducts shown in Fig. 7(D), which confirms "linkage" of the 1132 and 1108 cm^{-1} features. Thus, in this case the intensities of these two bands, relative to one another, remain similar to those observed in the 1:2:1 scrambled case, but intensities of both of them are proportionately decreased, relative to those associated with the $^{16}O_2$ and $^{18}O_2$ adducts.

2.1.2. The utility of coupling interactions as a structural probe

The previously discussed studies document and describe the spectral consequences of coupling interactions between ν(O–O) and internal modes of the trans-axial ligand. While it is obvious that such effects can severely complicate the RR spectra of these species, it is also true that such effects provide information which is not readily accessible by other methods. Specifically, the changes in spectral patterns which result from variations in coupling parameters are apparently greater than shifts in the inherent frequencies; i.e., slight structural perturbations which are insufficient to effect a change in vibrational frequency of the bound dioxygen are, in some cases, sufficient to induce an easily discernable change in the observed spectral pattern. Two separate studies are now summarized which nicely demonstrate this utility for detection of very subtle structural effects.

2.1.2.1. The effect of hydrogen bonding of (trans-axial) imidazole ligands on the observed spectral patterns. One control mechanism for the reactivity of heme proteins which has received considerable attention [72–76] involves alteration of the properties of the coordinated histydyl imidazole as a result of hydrogen bonding of the imidazole N–H to other active site residues or the peptide framework. The possible influence of such proximal side hydrogen bonding on the stability of O_2 adducts of Hb and Mb has been extensively discussed [72,75]. As will be seen, model compound studies clearly demonstrate the potential utility of vibrational coupling effects for revealing such subtle factors.

As will be made evident in the following discussion, the O_2 adducts of the imidazole complexes of cobalt porphyrins exhibit complicated RR spectral patterns characterized by multiple oxygen-isotope sensitive bands [77,78]. In this study we have employed the cobalt complex of a highly protected porphyrin (i.e., 5α,15α-bis[2-(2, 2-dimethylpropanamido)phenyl]-10α, 20α-(nonanediamidodi-*o*-phenylene) porphyrin, abbreviated $CoAz_{piv}\alpha\alpha$; its structure is shown later in the paper in Fig. 12) to eliminate the direct interaction between bound O_2 and other solution components. This facilitates selective modulation of the properties of the trans-axial bound imidazole by variation of solute conditions.

The RR spectrum of the $^{16}O_2$ adduct of $CoAz_{piv}\alpha\alpha$ exhibits two bands at 1158 and 1138 cm^{-1} (Fig. 8(A)). The spectrum of the $^{18}O_2$ adduct is shown in the same figure in trace B. In this case, the β-pyrrole deuteriated porphyrin was utilized to avoid overlap of the $\nu(^{18}O–^{18}O)$ with the porphyrin mode at 1078 cm^{-1}. As can be seen in trace B, two new bands appear at 1068 and 1082 cm^{-1}, the higher frequency band showing the greater intensity. Although the appearance of two bands in both traces A and B in the ν(O–O) region may suggest the presence of two structural conformers, the result shown in Fig. 8(C) demonstrates that this cannot be the correct interpretation. In this case (trace C) the solution contains the $^{16}O_2$, $^{18}O_2$ and $^{16}O^{18}O$ adducts (1:2:1 "scrambled" dioxygen). The strong symmetric band at 1111 cm^{-1} is readily assigned to $\nu(^{16}O–^{18}O)$; i.e., there is no evidence for the presence of a second conformer. Instead, the appearance of multiple bands discussed in traces A and B is the result of vibrational coupling of $\nu(^{16}O–^{16}O)$ and $\nu(^{18}O–^{18}O)$ with different internal modes of *coordinated* imidazole.

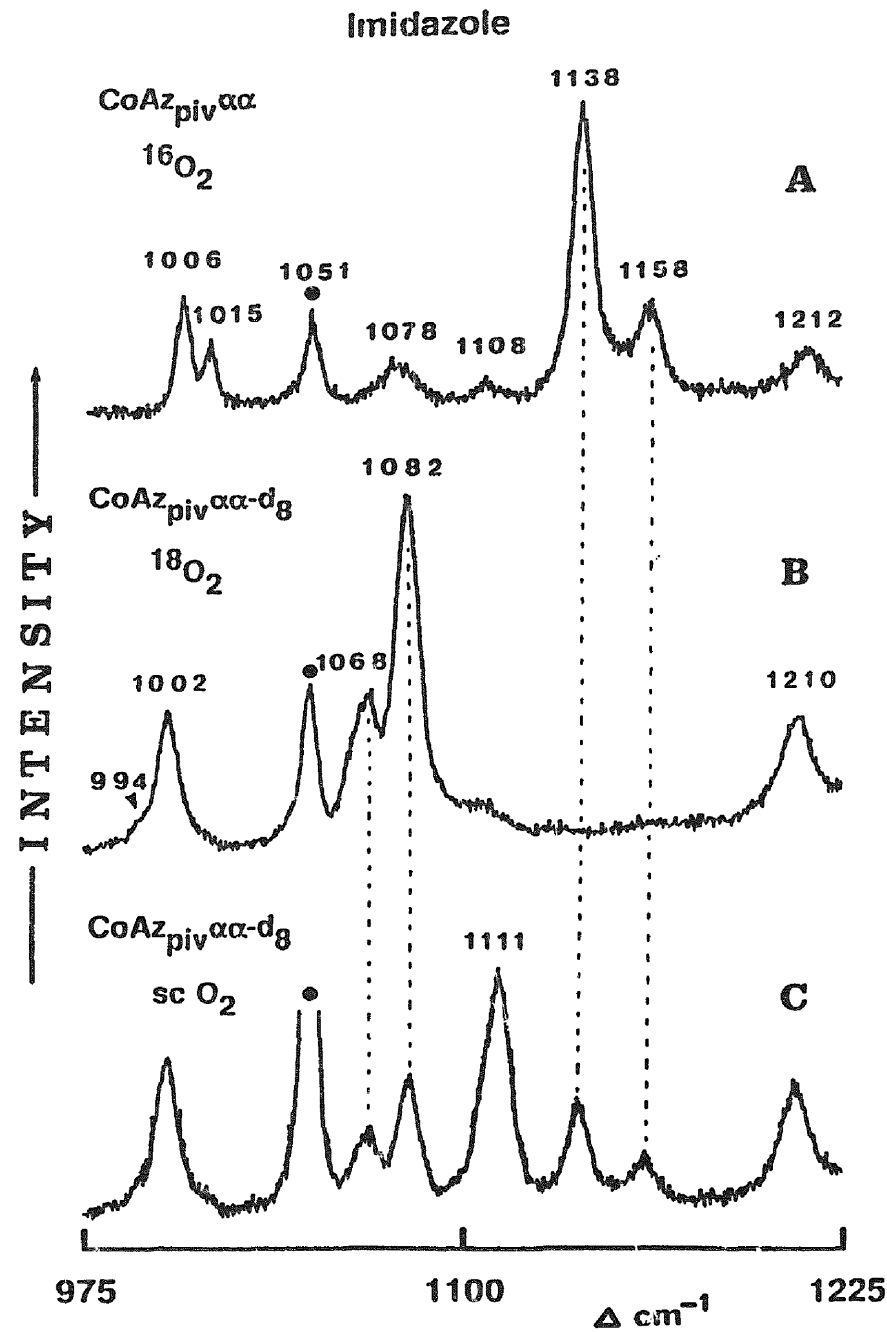

Fig. 8. Resonance Raman spectra of O_2 adducts of $CoAz_{piv}\alpha\alpha$ complex with imidazole. Excitation at 406.7 nm (~10 mW of laser power at the sample). The 1051 cm^{-1} band is due to $C^2H_2Cl_2$ (from Ref. [77]).

The validity of this interpretation was supported by comparison of the corresponding spectra obtained with deuteriated analogues of imidazole, where different vibrational patterns are observed for the adducts bearing axial ligated 4,5-dideuterioimidazole (Im-d_2) and 2,4,5-trideuterioimidazole (Im-d_3) [77]. The point is that these deuteriated imidazole analogues have identical chemical properties and therefore (in the absence of vibrational interaction) are expected to yield identical spectra. The complex behaviour observed in the RR spectra is thus the result of complicated vibrational mode coupling. Nevertheless, it is satisfying to point out that this complete set of complex data could be reasonably explained, in an internally consistent manner, by invoking vibrational coupling interactions among the specific modes of the various imidazole and O_2 isotopomer pairs.

Returning to analysis of the spectra in Fig. 8, approximation of the bound dioxygen as a harmonic oscillator leads to an expected isotopic shift of $\sim 66\ cm^{-1}$ ($\Delta\nu(^{16}O_2{-}^{18}O_2)$). That is, given a $\nu(^{16}O{-}^{18}O)$ inherent frequency of $1111\ cm^{-1}$, the $\nu(^{16}O{-}^{16}O)$ and $\nu(^{18}O{-}^{18}O)$ modes are expected to occur at 1144 and $1078\ cm^{-1}$, respectively. The spectrum of free imidazole exhibits a band near $1144\ cm^{-1}$ that is expected to shift up to $\sim 1150\ cm^{-1}$ upon coordination [79–81]; it was actually determined to be $1152\ cm^{-1}$ by comparison of more extensive data [77]. Interaction of the $\nu(^{16}O{-}^{16}O)$ mode (inherent frequency of $1144\ cm^{-1}$) with this mode results in the appearance of two bands shifted by $\sim 6\ cm^{-1}$ from their inherent frequencies; i.e., the 1144 and $1152\ cm^{-1}$ modes shift to 1138 and $1158\ cm^{-1}$. The lower frequency mode contains the major contribution of ν(O–O) and thus exhibits greater intensity.

The RR spectra presented in Fig. 8 were recorded in the presence of large excess of imidazole; ligand concentration $>100\times$ cobalt porphyrin concentration. At this high concentration in nonprotic solvents imidazole self-associates [82–84]. Thus, it is likely that spectra presented in this figure correspond to O_2 adducts in which the trans-coordinated imidazole is hydrogen bonded to excess imidazole present in the solution. Obviously, such interactions should be decreased or eliminated by increasing the temperature or lowering the concentration of imidazole. The interesting spectral patterns shown in Figs. 9 and 10 support this expectation.

In Fig. 9 are shown the spectra obtained for the $(^{16}O_2)CoAz_{piv}\alpha\alpha$(Im) complex in the presence of a slight excess of imidazole as a function of temperature. At 185 K the spectral pattern previously shown in Fig. 8(A) is observed; i.e., two RR bands are seen at 1138 and $1158\ cm^{-1}$ (trace A). However, at room temperature (trace D) these two bands have practically disappeared, and two new bands have emerged at 1127 and $1148\ cm^{-1}$. At the two intermediate temperatures (traces B and C), both sets of bands are observed. Essentially the same behavior is observed as the concentration of imidazole is varied while the concentration of cobalt porphyrin is kept constant (Fig. 10). At a base concentration of 1×10^{-2} M, the 1138 and $1158\ cm^{-1}$ doublet is dominant (trace A) while at 6×10^{-4} M the 1127/$1148\ cm^{-1}$ pair dominates (trace C). It is interesting to note that at very low imidazole concentrations (traces D and E) a base-free dioxygen adduct is apparently formed exhibiting the $\nu(^{16}O{-}^{16}O)$ at $1173\ cm^{-1}$, which shifts to $1107\ cm^{-1}$ upon $^{16}O_2/^{18}O_2$ isotopic substitution [78].

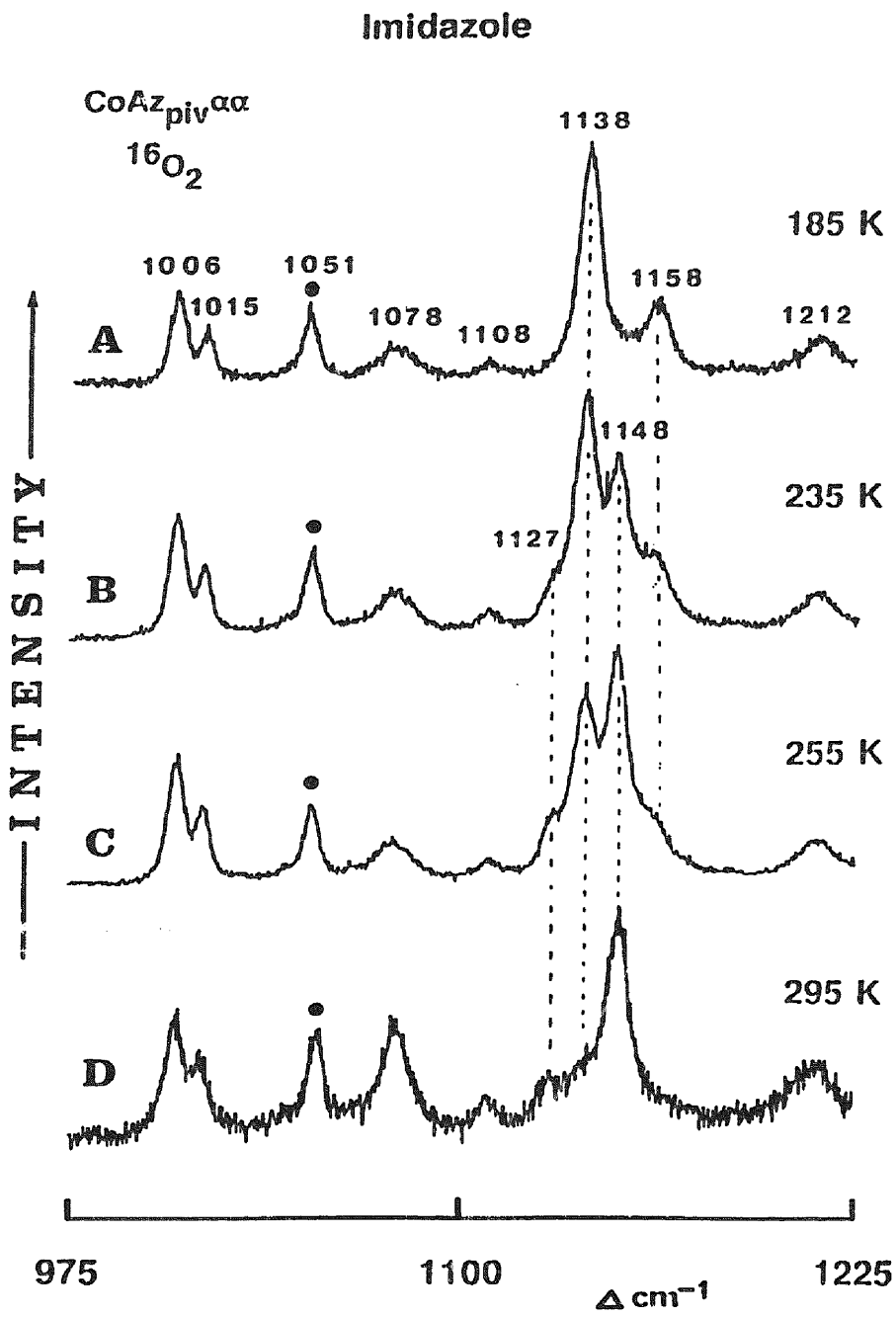

Fig. 9. Influence of temperature on resonance Raman spectra of the $^{16}O_2$ adduct of CoAz$_{piv}$αα complex with imidazole. Spectral conditions as in Fig. 8 (from Ref. [77]).

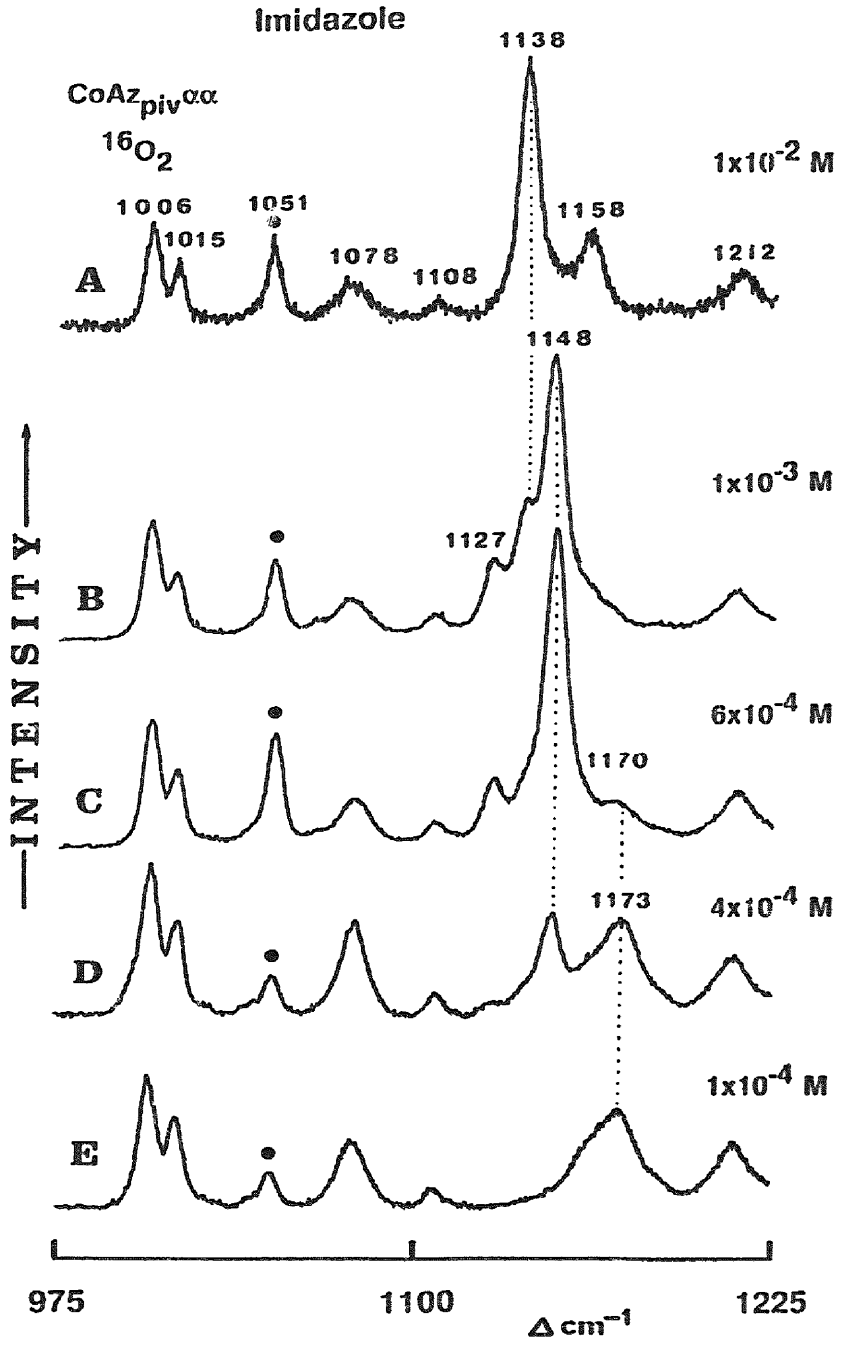

Fig. 10. Influence of imidazole concentration on resonance Raman spectra of the $^{16}O_2$ adduct of CoAz$_{piv}$αα complex with imidazole. Temperature at ~185 K. Spectral conditions as in Fig. 8 (from Ref. [77]).

The results presented in Figs. 9 and 10 indicate that the O_2 adduct that has a hydrogen-bonded imidazole axial ligand gives rise to the 1138/1158 cm^{-1} pair, while the non-hydrogen-bonded analogue is characterized by the 1127/1148 cm^{-1} pair of bands. To provide further support for this interpretation, we have included a study wherein a third solution component, which is known to form a strong hydrogen bond with imidazole [83], is added. The RR spectra shown in Fig. 11 demonstrate the effect of adding tri-*n*-octylphosphine oxide (TNOP) to a solution containing the $^{16}O_2$ adduct at low imidazole concentration. As is evident in the figure, the 1127/1148 cm^{-1} pair, characteristic of non-hydrogen-bound imidazole, is converted to the 1138/1158 cm^{-1} doublet upon addition of TNOP. Obviously, this behavior is consistent with the contention that the 1138/1158 cm^{-1} pattern is characteristic for the hydrogen-bonded imidazole dioxygen adduct.

The most reasonable interpretation of these two distinctly different spectral patterns is that the inherent frequencies of the interacting with $\nu(^{16}O–^{16}O)$ imidazole internal modes are different for the two types of ligated imidazole. Thus, the hydrogen-bonded form possesses an internal mode at 1152 cm^{-1} that couples with $\nu(^{16}O–^{16}O)$ at 1144 cm^{-1} giving rise to the pair of bands at 1138 and 1158 cm^{-1} (i.e., +6 and −6 cm^{-1} shifts, respectively). The observation of a strong 1148 cm^{-1} band along with a weak feature at 1127 cm^{-1}, indicates that the non-hydrogen-bonded axial imidazole possesses an internal mode having an inherent frequency of 1131 cm^{-1}. Interaction of this mode with the $\nu(^{16}O–^{16}O)$ mode at 1144 cm^{-1} gives rise to two bands at 1127 and 1148 cm^{-1} (i.e., shifted by −4 and +4 cm^{-1} from their inherent frequencies). It is also satisfying to note that, as expected (vidè infra), the strength of the observed coupling is greater for the former case where the inherent frequency difference is 8 cm^{-1} (1152–1144 cm^{-1}) than for the latter, where this difference is 13 cm^{-1} (1144–1131 cm^{-1}). That is, the observed frequency perturbations are 6 and 4 cm^{-1}, respectively, and the 1158/1138 cm^{-1} ratio is larger than the 1127/1148 cm^{-1} ratio. Finally, to conclude this section, it is important to emphasize that hydrogen bonding of one trans-axial imidazole with other solutes *does not* lead to changes in the inherent frequencies of the ν(O–O). The *only* spectral consequence of such hydrogen bonding is the change in the observed spectral pattern that results from alteration of vibrational coupling of ν(O–O) with internal modes of the trans-ligated imidazole.

2.1.2.2. Axial ligand distortions revealed by coupling effects. Another heme protein control mechanism which has attracted much attention, and which is rather difficult to probe, is the influence of steric-induced distortion of proximal histidine bonding to the heme. Though it is expected that vibrational spectroscopy would be an obviously useful probe of such effects, it has not proven possible to directly monitor the internal modes of histidine by ultraviolet RR methods and prospects do not seem hopeful [79–81]. Thus, the ability to probe internal modes of the proximal histidine indirectly via these coupling effects with ν(O–O), offers a unique opportunity. In order to assess this potential, a systematic study involving several different axial ligands (pyridine, imidazole and their derivatives) and several super-structured porphyrins (which are capable of inducing distortions in axial ligand disposition)

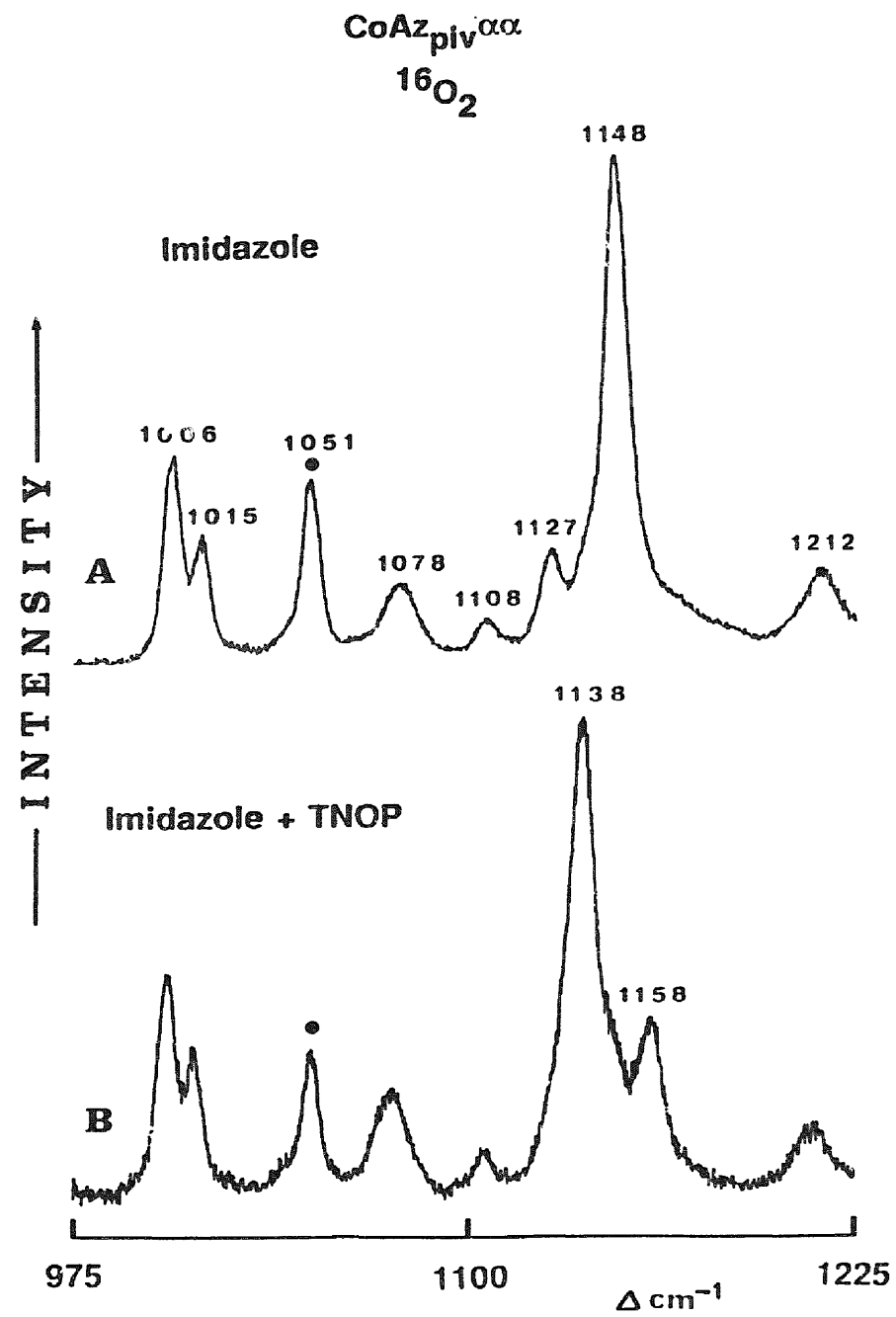

Fig. 11. Resonance Raman spectra of the $^{16}O_2$ adduct of CoAz$_{piv}$αα complex with imidazole. The effect of tri-*n*-octylphosphine oxide (TNOP); imidazole concentration $\sim 1 \times 10^{-3}$ M, TNOP concentration $\sim 5 \times 10^{-2}$ M. Temperature in both experiments ~ 185 K. Spectral conditions as in Fig. 8 (from Ref. [77]).

was undertaken [61]; the structures of the cobalt (II) complexes of the three superstructured porphyrins [39] utilized being given in Fig. 12.

As was shown earlier, an internal mode of pyridine, having an inherent frequency near 1070 cm^{-1} efficiently couples with $\nu(^{18}O-^{18}O)$ (Section 2.1.1.1). Thus, it is most convenient to concentrate attention on the $^{18}O_2$ adducts. The RR spectra of the $^{18}O_2$ adducts of the pyridine complexes with CoAz2 and CoDe2 are given in Fig. 13. As can be seen by comparison of traces A and B, an internal pyridine mode is observed at 1075 cm^{-1} (trace A). When pyridine-d_5 is used this band disappears and the inherent frequency of the $\nu(^{18}O-^{18}O)$ is revealed at 1086 cm^{-1} (trace B). This 2 cm^{-1} downshift of the $\nu(^{18}O-^{18}O)$ upon removal of the coupling implies that the inherent frequency of the internal coordinated pyridine mode is 1077 cm^{-1}; i.e.,

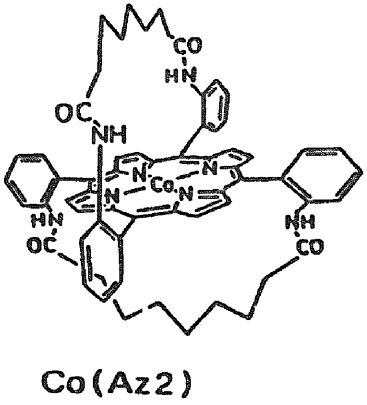

Co(Az2)

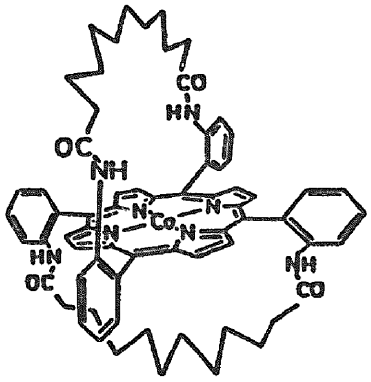

Co(De2)

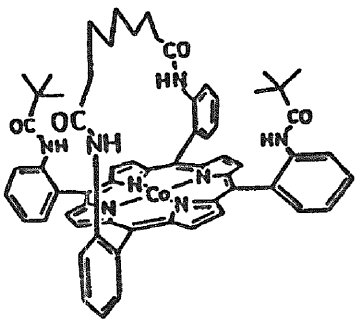

Co(Az-pivαα)

Fig. 12. Structures of Co(Az2), Co(De2) and Co($Az_{piv}\alpha\alpha$).

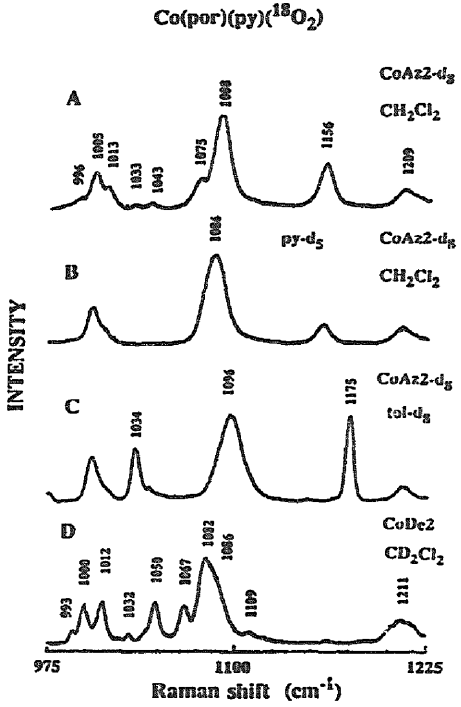

Fig. 13. Resonance Raman spectra of $^{18}O_2$ adducts of Co(porphyrin)(py) complexes (excitation at 406.7 nm): (A) CoAz2-d_8, CH_2Cl_2; (B) CoAz2-d_8, CH_2Cl_2; (C) CoAz2-d_8, tol-d_8; (D) CoDe2, CD_2Cl_2 (from Ref. [61]).

the inherent frequency is expected to be $2\,cm^{-1}$ higher than the observed $1075\,cm^{-1}$, given the $2\,cm^{-1}$ downshift of the $\nu(^{18}O–^{18}O)$. Thus, by comparison of Figs. 2(B) with 13(A), it is clear that the presence of the strap in the complex with CoAz2 imposes an encumbrance to trans-axial ligand binding which, in turn, induces a $+8\,cm^{-1}$ ($1077–1069\,cm^{-1}$) frequency perturbation of the internal mode of the bound pyridine.

In addition to the $8\,cm^{-1}$ upshift induced by the steric constrains of the strap, a detectable weakening in the strength of vibrational coupling is observed. Thus, as is shown in Fig. 13(C), when toluene-d_8 is used as the solvent, no satellite feature is observed in this region. The solvent-induced shift of $\nu(^{18}O–^{18}O)$ from $1086\,cm^{-1}$ (trace B) to $1096\,cm^{-1}$ (trace C) is comparable to that observed for analogous (unprotected) CoTPP adducts [84] and implies that the strap does not impede interaction of CH_2Cl_2 with the bound dioxygen. The essential point here is that, in the case of CoAz2, the bound pyridine is apparently sufficiently distorted to weaken vibrational coupling to such an extent that the two modes (1077 and $1096\,cm^{-1}$) are non-interacting. On the other hand, in the case of unrestrained pyridine bonding,

such as CoTPP(py)$^{18}O_2$ complex in toluene [84], coupling is observed between the 1067 and 1094 cm^{-1} modes.

The 8 cm^{-1} upshift of the pyridine mode is apparently caused by the steric hindrance between the strap and pyridine molecule that, in turn, influences the β(CCH) vibrations. In "unprotected" metalloporphyrins, such as CoTPP, the axial ligand is perpendicular to the mean porphyrin plane and tends to take the eclipsed orientation with respect to the N–Co–N axis [85]. In the case of the 9-carbon atom polymethylene strap (CoAz2) pyridine is too large to fit into the cavity. Surprisingly, such a distorted orientation of pyridine does not significantly influence the strength of the cobalt–oxygen linkage since the $\nu(Co–O_2)$ and $\nu(O–O)$ exhibit inherent frequencies similar to the dioxygen adducts of Co(T_{piv}PP) [84].

It is interesting to note that this apparent axial ligand distortion is relaxed in the case of the O_2 adducts with CoDe2, which possesses a longer, more flexible strap. As shown in Fig. 13(D), the $\nu(^{18}O–^{18}O)$ is observed at 1086 cm^{-1}, as a shoulder overlapped with the 1082 cm^{-1} porphyrin band and the internal pyridine mode again appears at 1067 cm^{-1} (inherent frequency of 1069 cm^{-1}).

Steric hindrance between the strap and the axial ligand also influences other physicochemical properties of metalloporphyrins. For example, Kyuno et al. [39] reported that the equilibrium constant values for pyridine and 1-methylimidazole (1-MeIm) binding to CoAz2 are about 100-fold less than those for CoDe2 or $CoAz_{piv}\alpha\alpha$ complexes. They pointed out that the binding of these nitrogeneous ligands is inhibited selectively in the case of CoAz2. Debois et al. [40] showed that iron(II) complexes of $CoAz_{piv}\alpha\alpha$, when reacted with 1-MeIm, formed mainly a 5-coordinate complex since the bulky pickets and a short strap restrict the axial ligand from binding inside the porphyrin "pocket". Thus, 1-MeIm binds from the "unprotected" side of the porphyrin plane. When the 9-carbon atom polymethylene strap is replaced by a 12-carbon atom strap, a 6-coordinate complex is formed; i.e., the size of the cavity is large enough to accommodate the axial ligand. They also reported that the $\nu(Fe–O_2)$ is practically insensitive to the strap length, a result which is consistent with cobalt complexes [60,61].

In conclusion, the relatively short strap of the CoAz2 complex causes distortion of the trans-axial ligand, while the longer, more flexible, strap of the CoDe2 porphyrin permits relatively unrestrained binding. The RR data not only show that the strength of the $Co–O_2$ linkage remains relatively unaltered by this distortion (i.e., the inherent frequencies for $\nu(O–O)$ remain constant), but they also provide definitive spectroscopic evidence for the distortion (i.e., the ligand internal modes are strongly perturbed and thereby give rise to remarkable spectral differences).

2.1.3. Quantitative treatment of the model compound data

The previous sections summarized the results for specific examples involving several different trans-axial ligands. While the existence of the coupling effect in each of these works was clearly demonstrated by isotopic substitution, in any given case the actual number of different coupling interactions was rather small and no attempt was made to relate the observed frequency shifts and relative intensity of the coupled modes to theory, although it was noted that the behavior generally

approximated that expected for coupled oscillators [67,68]. Having accumulated a relatively large body of data, it was then shown [71] that all of the different coupling interactions so far observed could be treated collectively and that the observed frequency shifts and relative intensities are in good agreement with the values calculated using the familiar Fermi resonance formulation [86].

2.1.3.1. Theoretical framework. As is fully described in a standard reference work on vibrational spectroscopy [87], anharmonicity may lead to interactions of normal modes giving rise to frequency perturbations of the coupled modes from their inherent frequencies and mixing of the vibrational eigenfunctions. Such interactions are adequately treated by first-order perturbation theory which leads to the following expression for the new frequencies. Here, we use a modification of Herzberg's notation.

$$\nu = \nu_{ni} \pm 1/2(4W_{ni}^2 + \delta^2)^{1/2} \tag{1}$$

In this expression

$$\nu_{ni} = 1/2(\nu_{ni}^\circ + \nu_i^\circ)$$

i.e., the average value of the unperturbed frequencies of the coupled modes.Also,

$$\delta = (\nu_n^\circ - \nu_i^\circ)$$

i.e., the separation of the unperturbed levels. Finally, W_{ni} is the matrix element of the perturbation function W in the equation

$$W_{ni} = \int \Psi_n^\circ W \Psi_i^\circ \, d\tau \tag{2}$$

where Ψ_n° and Ψ_i° are the nonperturbed eigenfunctions of the two vibrational levels which interact. W is determined by the anharmonic terms in the potential energy. Since Ψ_n° and Ψ_i° belong to the same symmetry and W is totally symmetric, these two levels will repel each other, each shifting by $1/2(4W_{ni}^2 + \delta^2)^{1/2}$ from the average value, and the shifts from the unperturbed values will increase as the separation decreases.

In Eq. (1), W_{ni} is an energy term which can be derived from known values of the perturbed and unperturbed frequencies (vidè infra). Such experimentally determined values of W_{ni} include a factor which depends on the effective mass of the coupled modes. Thus, in the case of the dioxygen adducts of interest here, the derived W_{ni} will depend on the reduced mass of the ν(O–O) and that of the internal ligand mode. Clearly, the relative W_{ni} values for $^{16}O_2$ coupling to different ligand modes *cannot* be easily estimated since there is ambiguity in defining effective reduced masses for internal modes. On the other hand, it is useful to consider the expected *relative* values of W_{ni} for coupling of different dioxygen isotopomers with the *same* internal ligand mode. Thus, while the inherent coupling strength is independent of the oxygen isotopomer employed, the experimentally determined W_{ni} values are

expected to vary in the following manner:

$$W_{ni}(^{16}O_2):W_{ni}(^{16}O^{18}O):W_{ni}(^{18}O_2)\approx 1.00:0.985:0.970$$

Utilization of these expected relative values is useful in calculating W_{ni} and the inherent (unperturbed) frequencies of ν(O–O) and internal ligand modes from the observed (i.e., perturbed) frequencies and intensities.

The vibrational interaction also leads to mixing of the eigenfunctions according to the following equations derived from perturbation theory [87]:

$$\Psi_n = a\Psi_n^\circ - b\Psi_i^\circ \tag{3a}$$

$$\Psi_i = b\Psi_n^\circ + a\Psi_i^\circ \tag{3b}$$

where

$$a = \sqrt{\frac{(4W_{ni}^2 + \delta^2)^{1/2} + \delta}{2(4W_{ni}^2 + \delta^2)^{1/2}}}$$

and

$$b = \sqrt{\frac{(4W_{ni}^2 + \delta^2)^{1/2} - \delta}{2(4W_{ni}^2 + \delta^2)^{1/2}}}$$

The above equations were derived for the interaction of a fundamental with an overtone or combination mode of the same symmetry to explain the appearance of two bands near 1300 cm^{-1} [$\nu(CO)_{sym}$] in the spectrum of CO_2 [86]. However, Lax [88] has shown that similar equations result for the coupling of two fundamentals in solids, and his approach has been applied to the analysis of Fermi resonance in fluid solution [89,90]. Later, Monecke [91] extended these treatments and has pointed out that, for frequencies and anharmonicities normally encountered in molecules, the new expressions yield calculated results which are insignificantly different from those calculated by using Eq. (1). Veas and McHale [69] have developed a general and rigorously correct theoretical framework for treating resonance vibrational interactions of solute modes with those of an unrestricted number (N) of associated solvent molecules. While this development represents an important contribution to the general problem of solute–solvent vibrational interactions (with no restrictions on N), for the special case where $N=1$, the equations are essentially identical with the Fermi resonance equations (i.e., Eq. (1), Eq. (3a) and Eq. (3b)). In fact, Veas and McHale [69] successfully applied their equations to the coupling of ν(O–O) with the DCP fragment of Co(TPP-d_8)(DCP)(O_2); i.e., the experimental data presented in Section 2.1.1.3.2.

2.1.3.2. Comparison of theory and experiment. In the cases presented here, difficulty arose in applying Eqs. (1), (2), (3a) and (3b) to the O_2 adducts of interest in that the inherent frequencies of the internal ligand modes are not directly available; i.e., the mode gains intensity only as a consequence of coupling with ν(O–O) and

only the *perturbed* frequencies were observed. In general, one cannot employ directly the frequency observed for the free ligand since coordination frequently shifts ligand modes by 10 cm^{-1} or more [61,62,79–81]. Thus, successful application of the theory to interactions of this type requires a more complete data set for a given adduct. That is, either the interaction must be removed (for example by selective deuteriation of the ligand) to reveal the inherent ν(O–O), or (at least two) oxygen isotopomers (each of which interacts with the *same* internal ligand mode) must be employed.

The observed relative intensities of the perturbed ν(O–O) and internal ligand modes can also be employed to help determine the coupling strength (W_{ni}) and inherent frequencies. Thus, in the case of the O_2 adducts discussed here, a resonance enhanced ν(O–O) mode interacts with a nonresonance enhanced internal axial ligand mode. The appearance of the internal ligand mode in the RR spectra is a consequence of mixing of the eigenfunctions and, accordingly, the intensity of the "mainly ligand" mode is expected to increase proportionally with b^2 (see Eq. (3b)). Similarly, the intensity of the "mainly ν(O–O)" mode will decrease relative to its unperturbed value, the fractional intensity being given by a^2 (see Eq. (3a)). It is emphasized that the *total* scattering intensity is not affected by the interaction but is merely distributed between coupled modes. For example, in the case of exact resonance, $\delta=0$, $a=b=(0.5)^{1/2}$, and it is seen that the perturbed levels are equal mixtures of Ψ_n° and Ψ_i°. In this particular case, wherein the inherent intensities of the ligand mode approaches 0, the result is that two bands of *equal* intensity are observed and these bands are shifted by equal magnitudes (in opposite directions) from their inherent (in this case, common) frequencies.

It is worth pointing out that in special situations (such as those discussed here) where an "inactive" mode gains intensity only by virtue of coupling with an active mode, the observed relative intensities, together with the observed (perturbed) frequencies, provide sufficient information to derive inherent frequencies and W_{ni} values. However, in practice, the small errors present in the experimental data lead to large uncertainties in the derived W_{ni} values and calculated inherent frequencies (more than 2 cm^{-1}). Utilization of multiple dioxygen isotopomers, taken together with the knowledge of the relative W_{ni} values for the various dioxygen isotopomers, provides additional restrictions on the combinations of inherent frequencies and W_{ni} values which will satisfy all of the above conditions (i.e., yield correct relative intensities and W_{ni} values of appropriate relative magnitudes).

Eqs. (1), (2), (3a) and (3b) were applied to data presented in Section 2.1.1. and 2.1.2 in the following manner. The observed and (estimated) inherent frequencies of both the ν(O–O) and axial ligand modes (for two or more dioxygen isotopomers) were used to calculate W_{ni} values and relative intensities with the use of a BASIC program based on Eq. (1) and Eqs. (3a) and (3b). The calculated intensities were then compared with those observed (integrated intensities) and the relative W_{ni} values were also available for comparison. Slight adjustments of the input data were made until calculated intensities matched those observed and W_{ni} values were of appropriate relative magnitude. During this fitting procedure, the perturbed (i.e., observed) frequency values which were used as input were maintained within experimental error of those actually observed. The value of the unperturbed ligand fre-

Table 1
Summary of observed and calculated R.R frequencies and intensities for model compounds

No.	Base	ν_o^i	ν_L^i	ν_L^i	Observed		Calculated		W_{ni}
					$\nu_o(I_o)$	$\nu_L(I_L)$	$\nu_o(I_o)$	$\nu_L(I_L)$	
	Co(TPP-d_8)								
1	4MI	$^{16}O_2$	1143	1108	1146(0.91)	1105(0.09)	1146(0.93)	1105(0.07)	10.68
2	4MI	$^{16}O^{18}O$	1110	1108	1121(0.57)	1099(0.43)	1119.5(0.55)	1098.5(0.45)	10.45
3	4MI	$^{18}O_2$	1077	1108	1074(0.92)	1111(0.08)	1074(0.92)	1111(0.08)	10.10
4	DCP	$^{16}O_2$	1156	1115	1160(0.91)	1112(0.09)	1159.4(0.93)	1111.5(0.07)	12.48
5	DCP	$^{16}O^{18}O$	1123	1115	1132(0.63)	1108(0.37)	1131.9(0.65)	1106(0.35)	12.36
6	DCP	$^{18}O_2$	1090	1115	1086(0.84)	1121(0.16)	1084.9(0.86)	1120(0.14)	12.25
7	Py	$^{18}O_2$	1081	1069	1084(0.88)	1067(0.12)	1084(0.83)	1066(0.17)	6.71
8	Py	$^{16}O^{18}O$	1114	1069	1115(0.93)	1067(0.07)	1115(0.98)	1068(0.02)	6.78
	Co($Az_{piv}\alpha\alpha$)								
9	Im	$^{16}O_2$	1144	1153	1138(0.75)	1158(0.25)	1139(0.74)	1158(0.26)	8.37
10	Im*	$^{18}O_2$	1078	1072	1082(0.68)	1068(0.32)	1082(0.71)	1068(0.29)	6.32
11	Im[a]	$^{16}O_2$	1144	1131	1148(0.84)	1127(0.16)	1148(0.81)	1127(0.19)	8.25
12	Im*	$^{18}O_2$	1078	1067	1082(0.71)	1063(0.29)	1082.5(0.76)	1063.5(0.24)	8.08
13	Im-d_1	$^{16}O_2$	1144	1150	1137(0.70)	1156(0.30)	1138(0.67)	1156(0.33)	8.49
14	Im-d_1^*	$^{18}O_2$	1078	1087	1076(0.85)	1089(0.15)	1076(0.85)	1089(0.15)	4.69
15	Im-d_2^*	$^{16}O^{18}O$	1111	1114	1106(0.62)	1119(0.38)	1106(0.62)	1119(0.38)	6.32
16	Im-d_3	$^{16}O_2$	1144	1117	1148(0.84)	1115(0.02)	1146(0.94)	1115(0.06)	7.62
17	Im-d_3^*	$^{16}O^{18}O$	1111	1117	1107(0.58)	1120(0.34)	1106(0.69)	1122(0.31)	7.42
18	Im-d_3	$^{16}O_2$	1114	1131	1148(0.84)	1127(0.14)	1147(0.84)	1128(0.16)	6.93
19	Im-d_3	$^{16}O^{18}O$	1111	1131	1107(0.58)	1132(0.08)	1109(0.92)	1133(0.08)	6.63

In all cases integrated intensities were used as observed intensities: asterisk indicates that Co($Az_{piv}\alpha\alpha$-d_8) was used for this case.
[a]Imidazole free from hydrogen bonding.

quency (an unknown quantity) was also varied, keeping the same value for the different O_2 isotopomers. In addition, the inherent ν(O–O) values were constrained by the reduced masses relationship; i.e., $\Delta\nu[^{16}O_2-(^{16}O^{18}O)] = \Delta\nu[(^{16}O^{18}O)-^{18}O_2] = 33\ cm^{-1}$.

The results of the application of this procedure to the O_2 adducts of Co(por)(base) are summarized in Table 1. Inspection of these data clearly demonstrates that all these complicated observed RR spectral patterns are precisely those predicted by using the computer program based on Eq. (1) and Eqs. (3a) and (3b). This excellent agreement between theory and experiment is illustrated diagrammatically in Fig. 14. The greater scatter at low values of ligand intensity, I_L, is merely the result of greater uncertainty in determining the experimental intensities of weak bands.

2.2. *Coupling of dioxygen with an associated solvent molecule*

2.2.1. *Methylene chloride*

As discussed in Section 2.1.1.1 (Fig. 2(A)), Bajdor et al. [60] obtained evidence for a peculiar type of vibrational coupling between the $\nu(^{16}O-^{16}O)$ of the bound

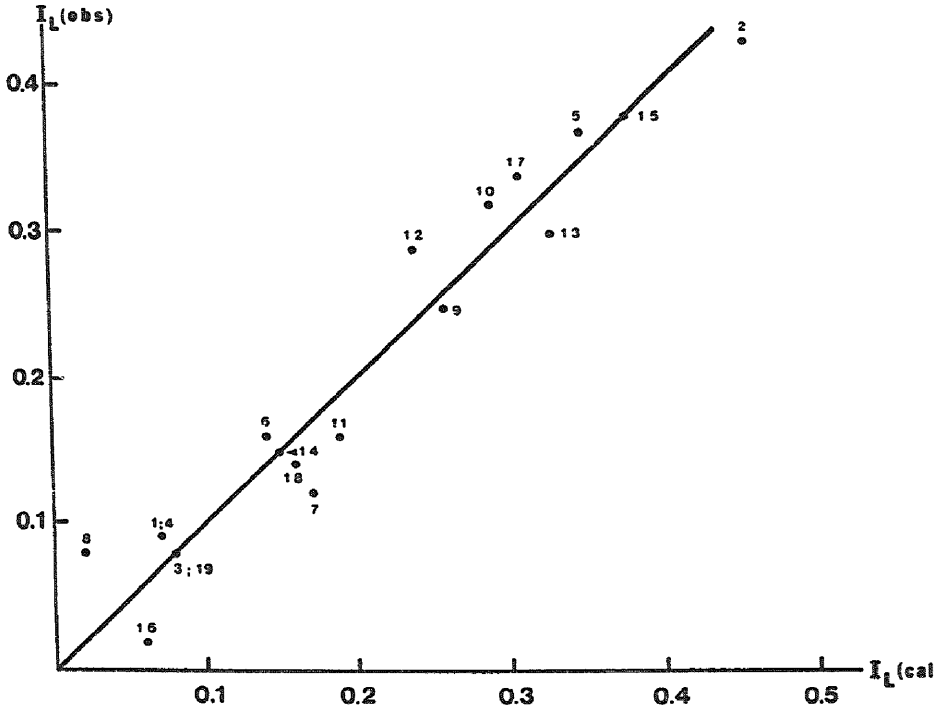

Fig. 14. Plot of observed versus calculated ligand intensity I_L (see Table 1 for numbering) (from Ref. [71]).

O_2 and an internal mode of solvent molecules (CH_2Cl_2) at $\sim$1156 cm^{-1}. Briefly, it was observed that the RR spectrum of Co(TPP-d_8) in a CH_2Cl_2 solution with added pyridine and $^{16}O_2$ exhibited two unresolved bands at $\sim$1155 and 1143 cm^{-1}. Upon solvent replacement with CD_2Cl_2, the 1155 cm^{-1} shoulder (which was assignable to an internal mode of the solvent) disappeared and, most significantly, the 1143 cm^{-1} band assigned to the $\nu(^{16}O–^{16}O)$ mode was shifted by 5 cm^{-1} to higher frequency. The displacement of the ν(O–O) from its inherent frequency of 1148 cm^{-1} is due to vibrational coupling, rather than to any possible chemical effects of the solvent change, since no similar shift was observed in the case of the $\nu(^{18}O–^{18}O)$ frequency. These experiments provided evidence of selective enhancement of the 1155 cm^{-1} band as a result of this coupling since this band was only very weakly observed in the experiment with $^{18}O_2$, though all components were present in comparable concentrations [60] for both the $^{16}O_2$ and $^{18}O_2$ cases. Comparison of RR spectra of the complexes in different solvents and the use of various porphyrins indicated that such coupling is facilitated by intimate association of a CH_2Cl_2 molecule (presumably via hydrogen bonding) with the bound O_2 [60].

2.2.2. Toluene

A more interesting case of selective enhancement of internal modes of associated solvent molecules is observed in the case of six-coordinate dioxygen adducts of cobalt porphyrins measured in toluene [60,84,92]. As can be seen in trace A of Fig. 15, two unresolved bands at 1151 and 1160 cm^{-1} are observed in the region where $\nu(^{16}O–^{16}O)$ is expected to occur. The appearance of two bands in this region is not due to the presence of two types of oxygen adducts since only one intense band is observed (at 1094 cm^{-1}) when $^{18}O_2$ is used (trace B). The weak band at 1067 cm^{-1} in this spectrum is due to enhancement of an internal mode of pyridine [60–62] as was shown earlier. The observation of a strong band at 1151 cm^{-1} in trace A is seen to be the result of a selective enhancement of an internal mode of toluene, because when toluene-$^2H_8$ is used instead of natural abundance toluene, only one strong band, assignable to $\nu(^{16}O–^{16}O)$, is observed at 1159 cm^{-1} (trace C). The small shoulder at 1174 cm^{-1} is due to an internal mode of the bulk solvent, toluene-$^2H_8$; i.e., its intensity is not enhanced relative to other solvent modes.

Natural abundance toluene exhibits three bands in this region at 1155, 1178 and 1210 cm^{-1} [63–65]. The relative intensities of these three bands in neat toluene are similar to those observed in Fig. 15(B); i.e., approximately 1:1:9. Thus, it is apparent that the occurrence of $\nu(^{16}O–^{16}O)$ in the vicinity of the internal modes of toluene gives rise to an enhancement of the 1178 and 1155 cm^{-1} toluene bands relative to the band observed at 1210 cm^{-1}. It is equally apparent that if the ν(O–O) is displaced to a much lower frequency by substitution of $^{18}O_2$, the bands corresponding to these internal modes are not enhanced significantly. Therefore, the mechanism by which the internal modes of the solvent molecules are selectively enhanced by interaction with ν(O–O) is critically dependent upon energy matching of the two sets of modes as explained in the previous section. The sensitivity of this energy matching was documented [84] by carrying out a set of experiments designed to "fine tune" the $\nu(^{16}O–^{16}O)$ so as to vary its frequency systematically between the two toluene modes at 1155 and 1178 cm^{-1}. Such variation was accomplished by employing a number of different nitrogeneous bases as the axial ligand. Since the bonding in these O_2 adducts can generally be formulated as $Co^{\delta+}–O_2^{\delta-}$, it is expected that the stronger is the axial ligand, the stronger the Co–O_2 bond and the weaker the O–O bond. Although other factors may be important, if these are held constant, the ν(O–O) should be sensitive to the nature (basicity) of the axial ligand. Indeed, the ν(O–O) was varied between 1169 and 1147 cm^{-1} as the pK_a of the particular pyridine derivative as the axial ligand varied between 0.67 and 9.70. As is clearly demonstrated in Fig. 16, the 1155 cm^{-1} toluene mode gains intensity, while the 1178 cm^{-1} mode experienced smaller and smaller enhancement relative to the 1210 cm^{-1}, as the ν(O–O) shifts from 1169 to 1147 cm^{-1}.

It is important to emphasize the fact that this type of vibrational coupling with "solvent" is actually the result of intimate association of an individual solvent molecule with the resonantly enhanced Co–O_2 fragment. This point is clearly demonstrated by the spectra given in Fig. 17. Trace A shows significant enhancement of the toluene modes (at ~1180 and 1153 cm^{-1}). As is shown in trace B, the spectrum of the dioxygen adduct of Co(T_{piv}PP)(4-cyanopyridine), obtained under identical

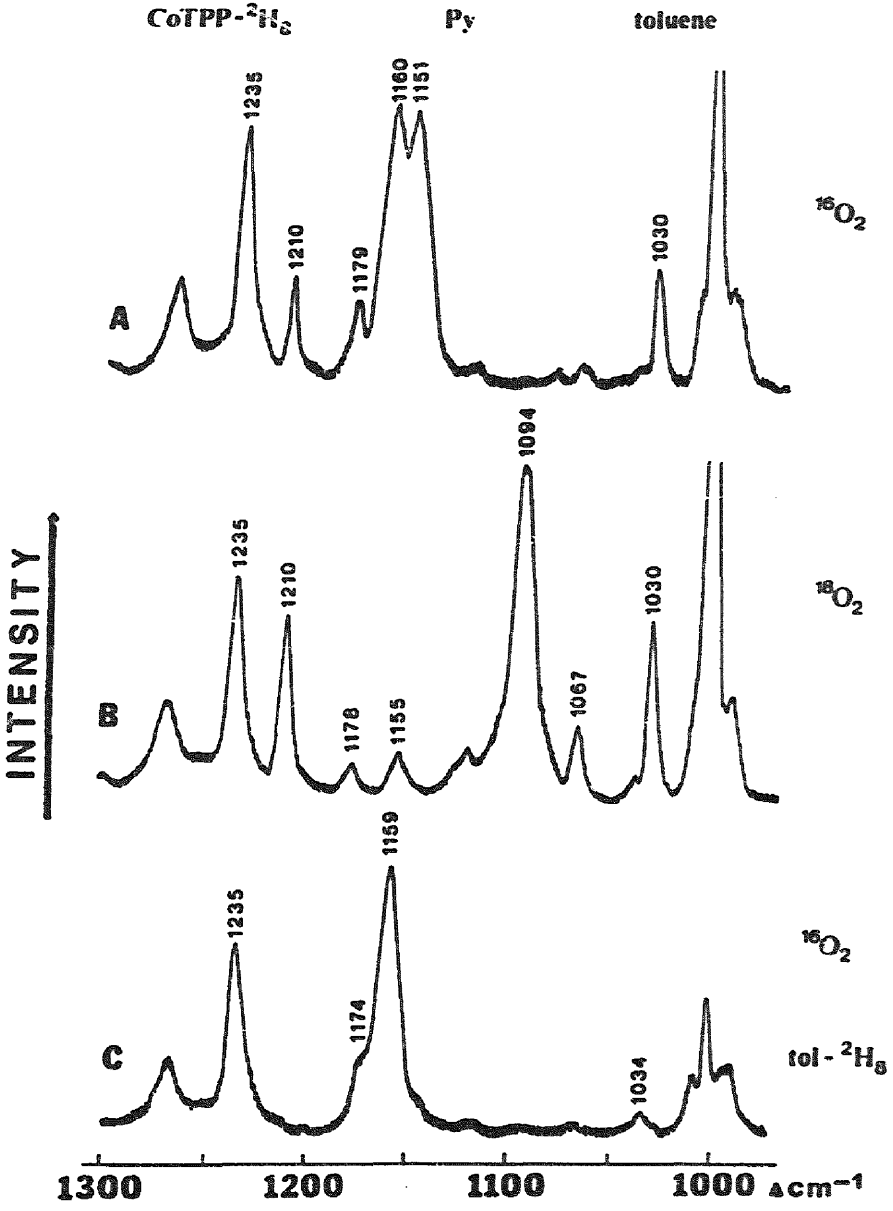

Fig. 15. Resonance Raman spectra of Co(TPP-$^2H_8$) in toluene containing 3% pyridine at −85°C under ~4 atm of O_2 pressure: (A) $^{16}O_2$; (B) $^{18}O_2$; (C) $^{16}O_2$, toluene-$^2H_8$ (from Ref. [84]).

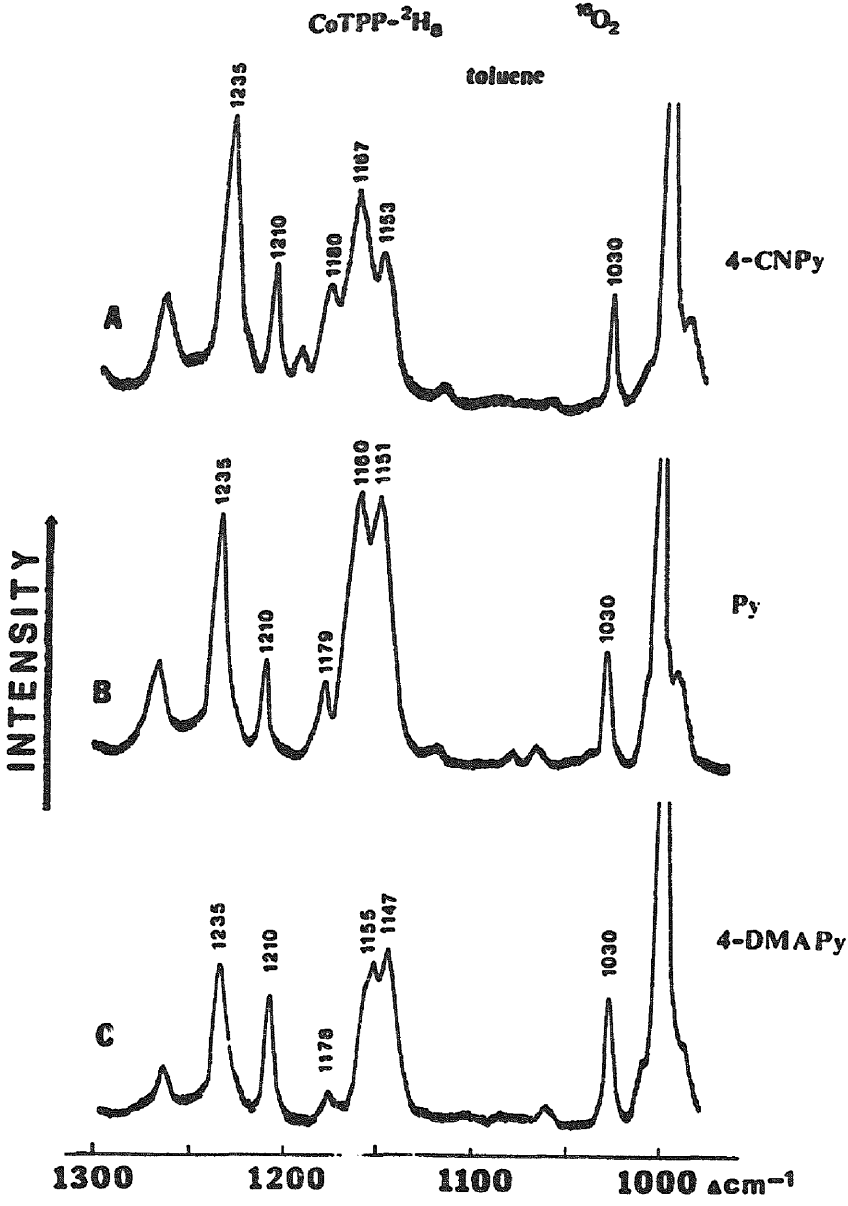

Fig. 16. Resonance Raman spectra of Co(TPP-$^2H_8$) in toluene containing 3% 4-cyanopyridine (A), pyridine (B), and 4-dimethylaminopyridine (C) at −85°C under ~4 atm of $^{16}O_2$ pressure (from Ref. [84]).

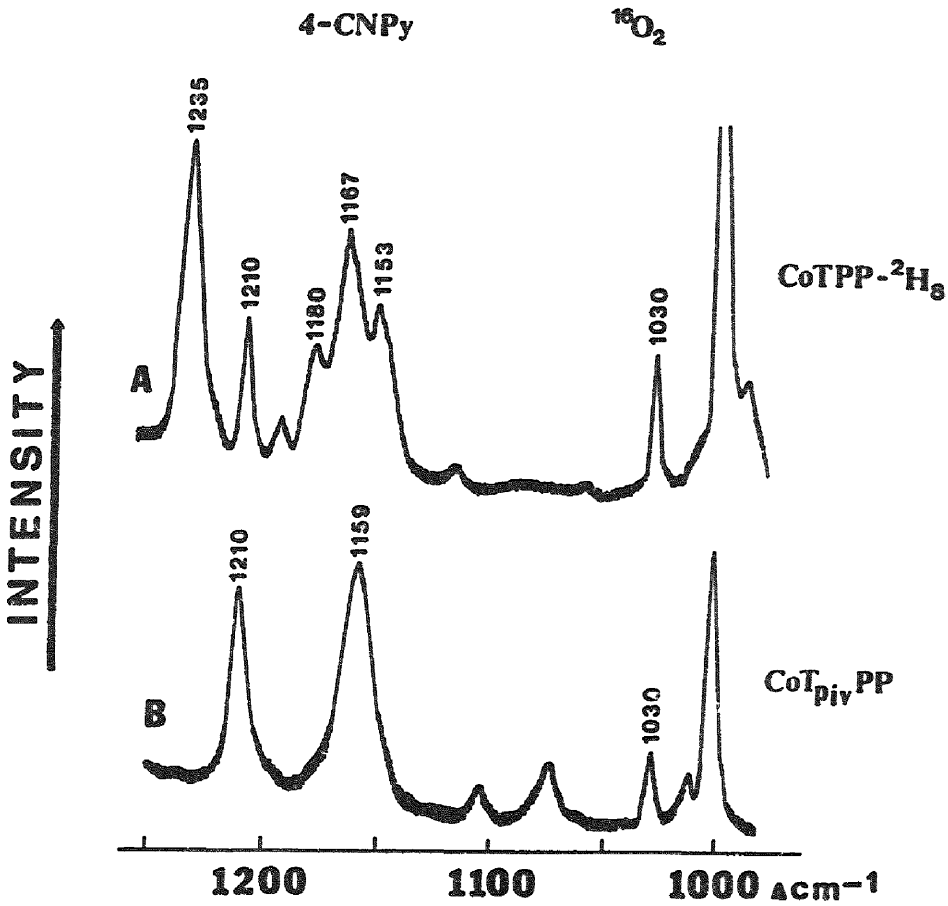

Fig. 17. Resonance Raman spectra of Co(TPP-$^2H_8$) (trace A) and α^4-Co(T_{piv}PP) (trace B) in toluene containing 3% 4-cyanopyridine at −85°C under ~4 atm of $^{16}O_2$ pressure (from Ref. [84]).

conditions, exhibits only one strong band at 1159 cm^{-1}. This latter porphyrin is a (so-called) super-structured porphyrin which possesses bulky pivaloyl groups on one side only of the macrocycle. It is generally accepted that these groups restrict close association of all but very small molecules with the bound molecular oxygen. Clearly, restricted access of the toluene molecule to the bound O_2 prevents the vibrational coupling interaction and eliminates selective enhancement of the solvent modes. In a later study by Nakamoto and co-workers [92], other atropisomers of such super-structured porphyrins were employed to show that, as this restriction is incrementally lifted (by using macrocycles with 4, 3 or 2 bulky groups on one side), the coupling interaction is restored.

3. Applications to heme proteins

3.1. Dioxygen adducts of cobalt-substituted hemoglobin and myoglobin

The concepts and quantitative treatment (Section 2.1.3.1) outlined above for analysis of these complex vibrational interactions can, in principle, be applied to the RR spectra of the O_2 adducts of heme protein systems. However, it must be pointed out that such attempts are naturally somewhat hindered by the inability to eliminate or control the vibrational coupling as was accomplished in the studies of the model compounds.

Thus in the model systems, fully deuteriated ligands can be used to reveal the inherent ν(O–O) and deuteriated porphyrins (e.g., Co(TPP-d_8)) can be employed to remove overlapping macrocycle modes. Such manipulations are not easily accomplished in the case of protein systems. In addition, the inherent frequencies of the internal modes of the coordinated histidylimidazole fragment are not known since conditions for direct resonance enhancement of these have not been identified. While systematic application of the procedure to the proteins is thus hampered by the considerations outlined above, it is satisfying to point out that the observed frequencies and intensities can be closely approximated with Eqs. (1), (2), (3a) and (3b) by making several assumptions which are *well-supported* by existing data.

The RR spectra of six different cobalt-substituted oxyheme proteins (Hb_{Co}, Mb_{Co}, α_{Co}, β_{Co}, $\alpha_{Fe}\beta_{Co}$, and $\alpha_{Co}\beta_{Fe}$) were first presented and discussed qualitatively in an early work [67]. The spectral data for Hb_{Co} was later analyzed quantitatively [71] by the method outlined in Section 2.1.3.1 and this analysis is briefly summarized below.

The RR spectra of the $^{16}O_2$, $^{16}O^{18}O$, and $^{18}O_2$ adducts of Hb_{Co} measured in aqueous and deuteriated (D_2O) buffers are presented in Fig. 18. In order to clarify the complicated multiple interactions, we have diagrammatically represented the observed spectra in Fig. 18, including separate sets of vertical lines for each component of the spectrum (i.e., sets for the histidine and ν(O–O) modes). In the figure, the *inherent* (i.e., unperturbed) frequencies of coordinated histidine and dioxygen are depicted with dotted and broken lines, respectively, while the solid lines represent the calculated *perturbed* frequencies. It should be noted that this diagram is not intended to provide an accurate representation of the calculated relative intensities. Those are listed in Table 2.

As was shown in our earlier work [71], these complicated spectral patterns, including the observed RR frequencies and their approximate relative intensities are, in fact, precisely those predicted by Eq. (1) and Eqs. (3a) and (3b), given the following few, well supported, assumptions. There is *only one* O_2 conformer

Fig. 18. Resonance Raman spectra of cobalt-substituted hemoglobin A, Hb_{Co}, in 50 mM Tris–HCl buffer (H_2O or ^2H_2O) pH (pD) 8.2, excitation at 406.7 nm. Vertical lines represent the following: dotted (· · ·), inherent frequencies of coordinated histidine; broken (- - -), inherent frequencies of coordinated O_2; and solid lines (———), calculated perturbed frequencies of coordinated O_2 and histidine (from Ref. [71]).

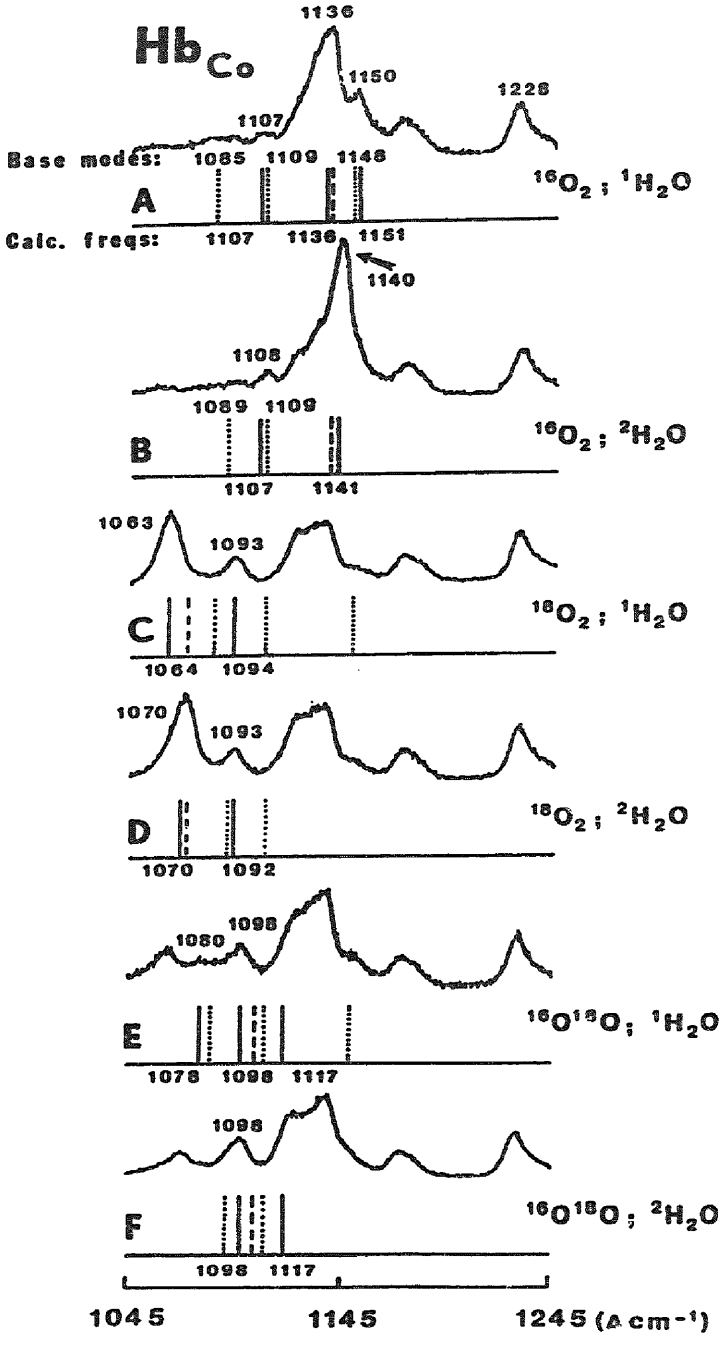
Hb Co
1136
1150
1228
1107
Base modes: 1085 1109 1148
A
$^{16}O_2$; $^{1}H_2O$
Calc. freqs: 1107 1136 1151
1140
1108
1089 1109
B
$^{16}O_2$; $^{2}H_2O$
1107 1141
1063
1093
C
$^{18}O_2$; $^{1}H_2O$
1064 1094
1070
1093
D
$^{18}O_2$; $^{2}H_2O$
1070 1092
1098
1080
E
$^{16}O^{18}O$; $^{1}H_2O$
1078 1098 1117
1098
F
$^{16}O^{18}O$; $^{2}H_2O$
1098 1117
1045
1145
1245 (Δ cm^{-1})

Table 2
Observed and calculated RR frequencies and intensities for cobalt-substituted oxyhemoglobin in H_2O and ^2H_2O

O_2 isotopomer	ν_o^i	ν_L^i	Observed		Calculated		W_{ni}
			$\nu_o(I_o)$	$\nu_L(I_L)$	$\nu_o(I_o)$	$\nu_L(I_L)$	
(1) $^{16}O_2$	1139	1148	1136(0.86)[a]	1150(0.14)[a]	1136(0.80)	1151(0.2)	6.00
(2) $^{16}O_2$	1139	1109	—[b]	1107(weak)	1141(0.94)	1107(0.06)	9.52[d]
(3) $^{16}O^{18}O$	1106	1109	1098(?)	—[c]	1098(0.58)	1117(0.42)[b]	9.38
(4) $^{16}O^{18}O$	1106	1085	—[b]	1080(weak)	1113(0.80)	1078(0.20)[b]	13.96[d]
(5) $^{18}O_2$	1073	1085	1063(0.78)	1093(0.22)	1064(0.70)	1094(0.30)	13.75
(6) $^{16}O_2$	1139	1109	1140(?)	1108(weak)	1141(0.94)	1107(0.06)	9.52[e]
(7) $^{16}O^{18}O$	1106	1109	1098(?)	—[c]	1098(0.58)	1117(0.42)	9.38[e]
(8) $^{16}O^{18}O$	1106	1089	—[b]	—[b]	1109(0.87)	1086(0.13)	7.67[d]
(9) $^{18}O_2$	1073	1089	1070(0.79)	1093(0.21)	1070(0.86)	1092(0.14)	7.55

In all cases integrated intensities were used as observed intensities. Entries 1–5 obtained from H_2O solution, entries 6–9 obtained from ^2H_2O solution.
[a]Intensity calculated from data in Ref. [15].
[b]These features derived from a second interaction. Observed features are determined by the primary interaction.
[c]Band obscured by overlap with porphyrin macrocycle mode.
[d]Calculated frequencies and intensities were obtained using W_{ni} values derived from the W_{ni} value of the corresponding dioxygen isotopomer (e.g., 9.52 obtained as $9.38 \times 1.0/0.985$).
[e]The frequencies and intensities are calculated using the same W_{ni} as was used for H_2O (i.e., 9.52).

present whose inherent ν(O–O) frequencies are: $\nu(^{16}O–^{16}O) = 1139\ cm^{-1}$, $\nu(^{16}O–^{18}O) = 1106\ cm^{-1}$, and $\nu(^{18}O–^{18}O) = 1073\ cm^{-1}$ (note the enforced agreement of the dioxygen isotopic shift of $33\ cm^{-1}$). The histidylimidazole fragment possesses internal modes at 1148, 1109, and $1085\ cm^{-1}$ in H_2O, but upon exchange (NH/ND) in D_2O the first two modes are downshifted to 1109 and $1089\ cm^{-1}$, respectively, while the $1085\ cm^{-1}$ mode moves down below $1045\ cm^{-1}$. These assumed histidylimidazole modes are entirely consistent with previously reported data [93,94]. Thus, free histidine in H_2O (pH 8.2) exhibits four bands in this region: 1158 (broad), 1108, 1093, and $1070\ cm^{-1}$. In D_2O, only two bands, at $1097\ cm^{-1}$ (strong) and $1107\ cm^{-1}$ (weak), are observed in this same range. All of these modes are apparently of A′ symmetry, thus they can couple with the ν(O–O) mode [93,94]. As has been previously demonstrated [79–81], these histidylimidazole modes may shift slightly upon coordination.

Hydrogen bond formation between bound dioxygen and the distal histidyl NH is now generally accepted as a potentially important factor in the control of O_2 binding [6–13]. As was made clear in our work published earlier [67,71], H_2O/D_2O exchange (which leads to NH/ND exchange of the proximal, as well as the distal, histidylimidazole fragments) may differentially alter the vibrational interaction between the various ν(O–O) isotopomers and the internal modes of the proximal histidylimidazoles, which results in a wide variation in observed RR spectral patterns and apparent "shifts". To the extent that such "shifts" cannot then be unambiguously ascribed to

changes in distal side hydrogen bond strength, they cannot be taken as evidence for distal side hydrogen bonding, as had been proposed in an early study of the RR spectra of oxygenated adducts of cobalt-substituted heme proteins [95]. However, we wish to emphasize that the interpretation which invokes vibrationally coupled dioxygen does not imply that distal side hydrogen bonding is nonexistent, but simply that the observed H_2O/D_2O shifts are the result of altered vibrational coupling patterns rather than altered hydrogen bond strengths [60,67,71,77,78].

3.2. Dioxygen adducts of cytochrome P450: coupling of ν(O–O) with the internal mode of the substrate

As is discussed in Section 2.2, internal modes of solvent or other solute molecules can be resonance enhanced by specific association and interaction with the bound dioxygen. This enhancement requires close association of the molecule in question with the bound dioxygen, and is critically dependent upon energy matching of the mode with the ν(O–O). The RR spectra of the dioxygen adduct of adamantanone-bound cytochrome P450 from *Pseudomonas putida* [96] provide an interesting example of selective enhancement of the internal modes of an enzyme-bound substrate molecule.

Cytochromes P450 is a family of heme monooxygenase enzymes involved in a variety of oxidative reactions [97]. Among various cytochromes P450, the one isolated from the bacterium *Pseudomonas putida* is induced by camphor and is known as cytochrome $P450_{cam}$. It has been the most extensively studied member of this class of enzymes owing to its relative ease of handling and its ready availability [97]. This cytochrome is the terminal oxidase in the *d*-camphor hydroxylase system and catalyzes hydroxylation of this substrate with exquisite regio- and stereospecificity; i.e., the substrate is held in a fixed position near the (hydroxylating) heme active site. The molecular structure of $P450_{cam}$ has been well established [97–101]. Unlike the majority of other heme proteins, which utilize histidylimidazole as an axial ligand, cytochrome $P450_{cam}$ possesses thiolate (Cys357) as the proximal axial ligand that binds to the heme iron. In the substrate-free form, a cluster of water molecules occupies the substrate pocket, one of which serves as the distal-side axial ligand. Upon the binding of camphor, the water cluster is expelled from the substrate binding site and the heme assumes a pentacoordinated, high-spin configuration. The substrate is in close proximity to the heme iron on the distal side and is held in a relatively fixed position by a hydrogen bonding interaction between its carbonyl oxygen and the hydroxyl group of the side chain Tyr96. In addition, there is a "lock-and key" hydrophobic interaction between the camphor *gem*-dimethyl groups and Leu244 and Val295. Thus, the substrate is positioned in the enzyme active site in a way that it can interact with a molecular oxygen molecule that binds to the heme iron at the distal side [97–101].

Figs. 19 and 20 show the RR spectra of dioxygen adducts of camphor- and adamantanone-bound cytochrome $P450_{cam}$. Comparison of these figures illustrates the effect of substrate replacement on the ν(O–O) mode. It is emphasized that the electronic absorption spectrum and heme RR core vibrations of the dioxygen adducts

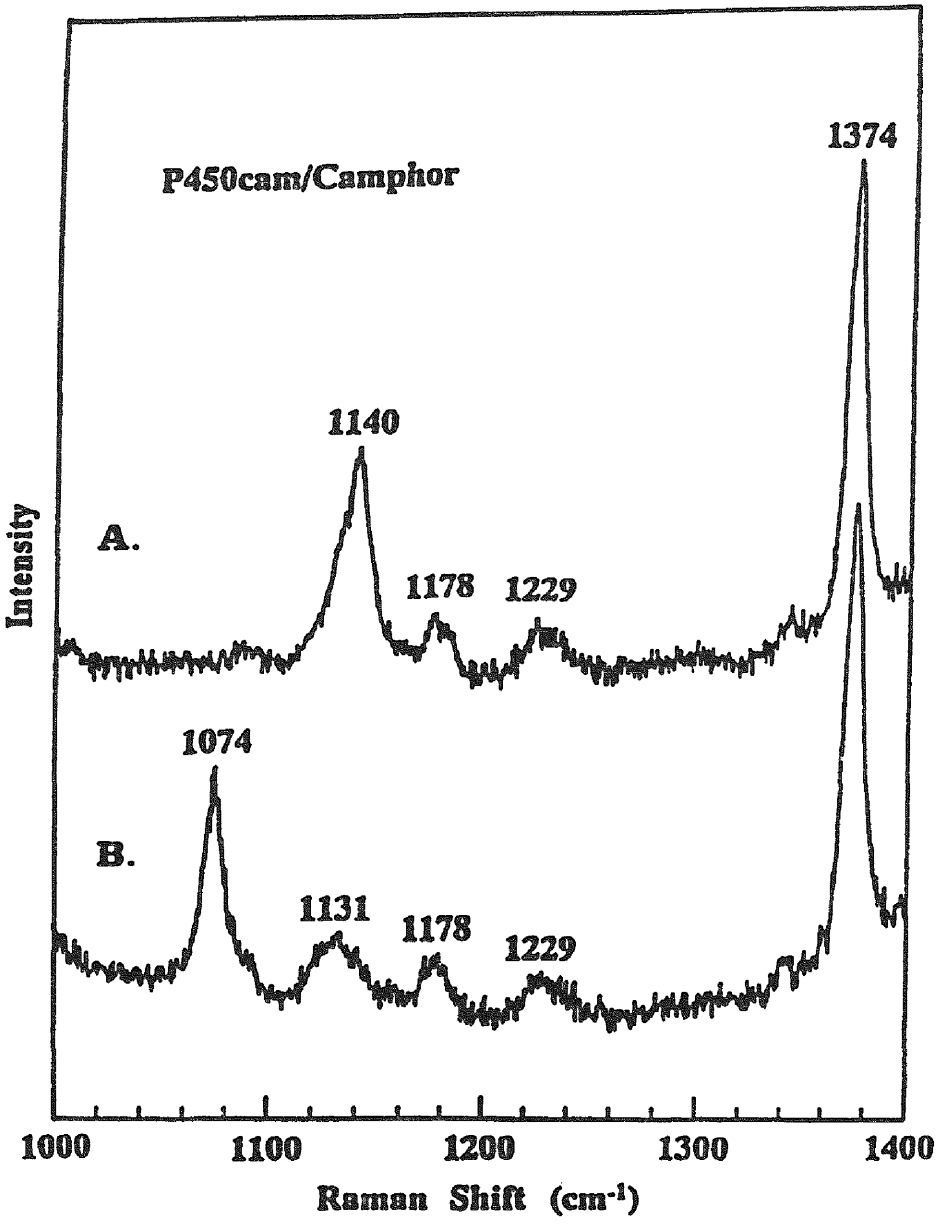

Fig. 19. Resonance Raman spectra of dioxygen adduct of camphor-bound cytochrome $P450_{cam}$ in the ν(O–O) region: trace A, $^{16}O_2$; trace B, $^{18}O_2$. Excitation at 413.1 nm (from Ref. [96]).

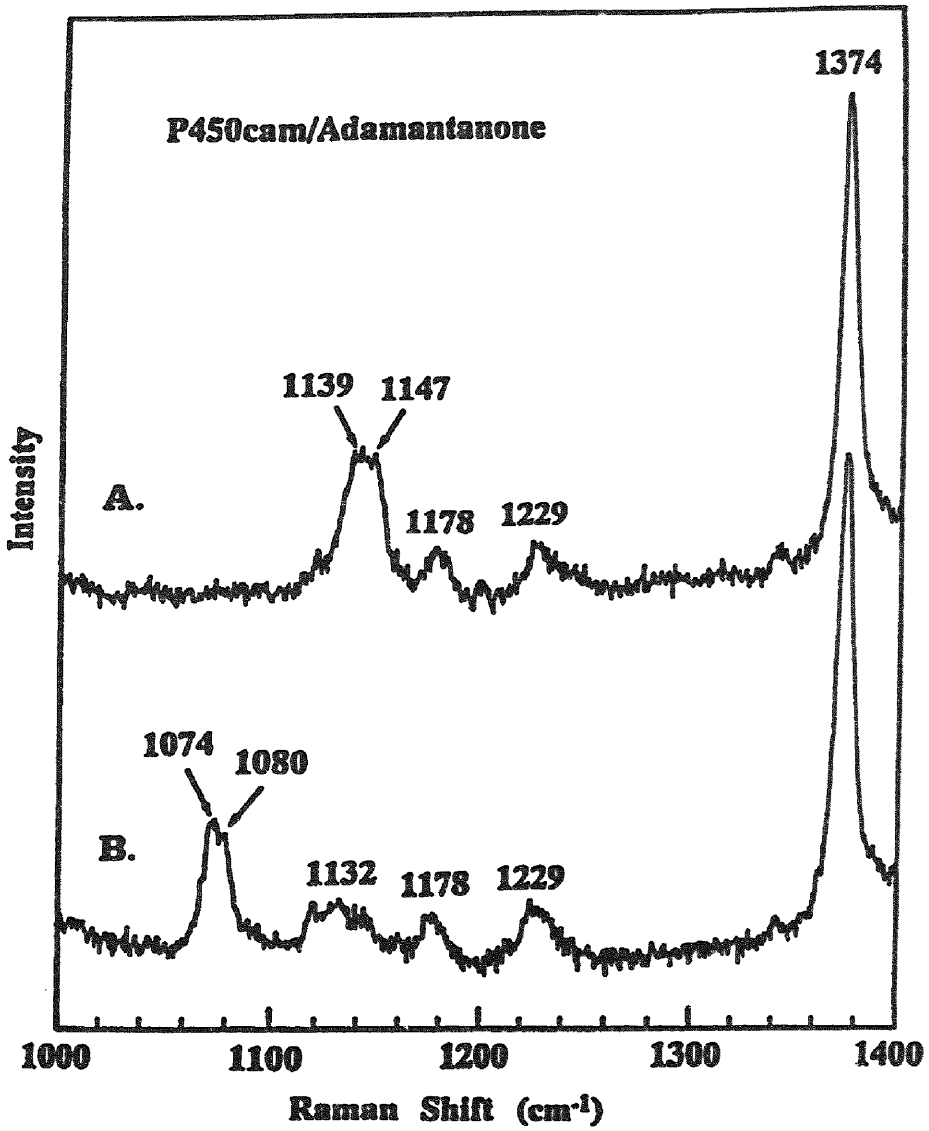

Fig. 20. Resonance Raman spectra of dioxygen adduct of adamantanone-bound cytochrome $P450_{cam}$ at −80°C in the ν(O–O) region: trace A, $^{16}O_2$; trace B, $^{18}O_2$. Excitation at 413.1 nm (from Ref. [96]).

are identical for both substrates [96]. However, the spectral pattern in the ν(O–O) region exhibits a dramatic change. While a single strong band is observed at 1140 cm^{-1} in Fig. 19(A), in Fig. 20(A), two bands of nearly equal intensity are

observed at 1139 and 1147 cm^{-1}. The assignment of these bands to the $\nu(^{16}O–^{16}O)$ mode is confirmed by the shifts observed upon $^{16}O_2/^{18}O_2$ substitution (traces B of Figs. 19 and 20). The magnitudes of the observed isotopic shifts (67 and 65 cm^{-1}, respectively) are in good agreement with those expected for the diatomic harmonic oscillator (i.e., 65 cm^{-1}).

Fig. 21 shows the difference spectra of the $^{16}O_2$ and $^{18}O_2$ adducts of cytochrome $P450_{cam}$ in the presence of camphor (trace A) and adamantanone (trace B) [96]. These spectra give a clear-cut comparison of the band intensities and widths of the ν(O–O) modes for both substrate-bound adducts, because the interfering heme modes are cancelled out. The $\nu(^{16}O–^{16}O)$ and $\nu(^{18}O–^{18}O)$ of $P450_{cam}$ are observed, at 1140 cm^{-1} (positive peak) and 1074 cm^{-1} (negative peak), as symmetric RR bands; an observation that is in agreement with data presented in early work on these systems [102–104]. In trace B of Fig. 21 it is noted that both the $\nu(^{16}O–^{16}O)$ and $\nu(^{18}O–^{18}O)$ are broader (each is a doublet at 1139/1147 and 1074/1080 cm^{-1}, respectively) for the adamantanone-bound adduct, relative to camphor. These multiple lines can be attributed to the known conformational disorder [99] of the Fe–O_2 linkage caused by different orientations of adamantanone within the heme pocket [96]. However, it is especially important to note that, in addition to the broadening caused by the multiple conformers, the bandwidth of the unresolved features in the ν(O–O) region of the $^{16}O_2$ adduct of the adamantanone-bound enzyme is significantly broader than that of the $^{18}O_2$ adduct, though the integrated areas of the positive and negative peaks are identical within experimental error. The observation of selective band broadening of *only one* isotopomer ($^{16}O_2$) is most reasonably ascribed to a vibrational coupling interaction and enhancement of an internal mode of the bound adamantanone. As is seen in trace C, several Raman bands occur in this region; in particular, the mode at 1140 cm^{-1} is closely energy-matched with the $\nu(^{16}O–^{16}O)$ frequency. The natural substrate, camphor, does not exhibit any band in this region and no evidence of a perturbed spectral pattern is indicated in trace A.

As we discussed in a previous section (Section 2.2), RR enhancement of the solvent or solute molecule internal mode *via* such vibrational coupling interactions requires close association of the molecule in question with the bound dioxygen and is critically dependent upon energy matching of the mode with ν(O–O). Clearly, these two requirements are satisfied for the dioxygen adduct of adamantanone-bound cytochrome P450, and may be responsible for the observed band broadening in the case of $^{16}O_2$ adduct, although further studies (employing deuteriated substrate) would be needed to unambiguously confirm such coupling.

Fig. 21. Differennce RR spectra of the $^{16}O_2$ and $^{18}O_2$ adducts of cytochrome P450 from *Pseudomonas putida* in the presence of camphor (trace A) and adamantanone (trace B) obtained by normalizing the respective RR spectra to the 1374 cm^{-1} band. Trace C: Raman spectrum (413.1 nm excitation) of adamantanone dissolved in CH_2Cl_2. The solvent band at 1157 cm^{-1} is subtracted (from Ref. [96]).

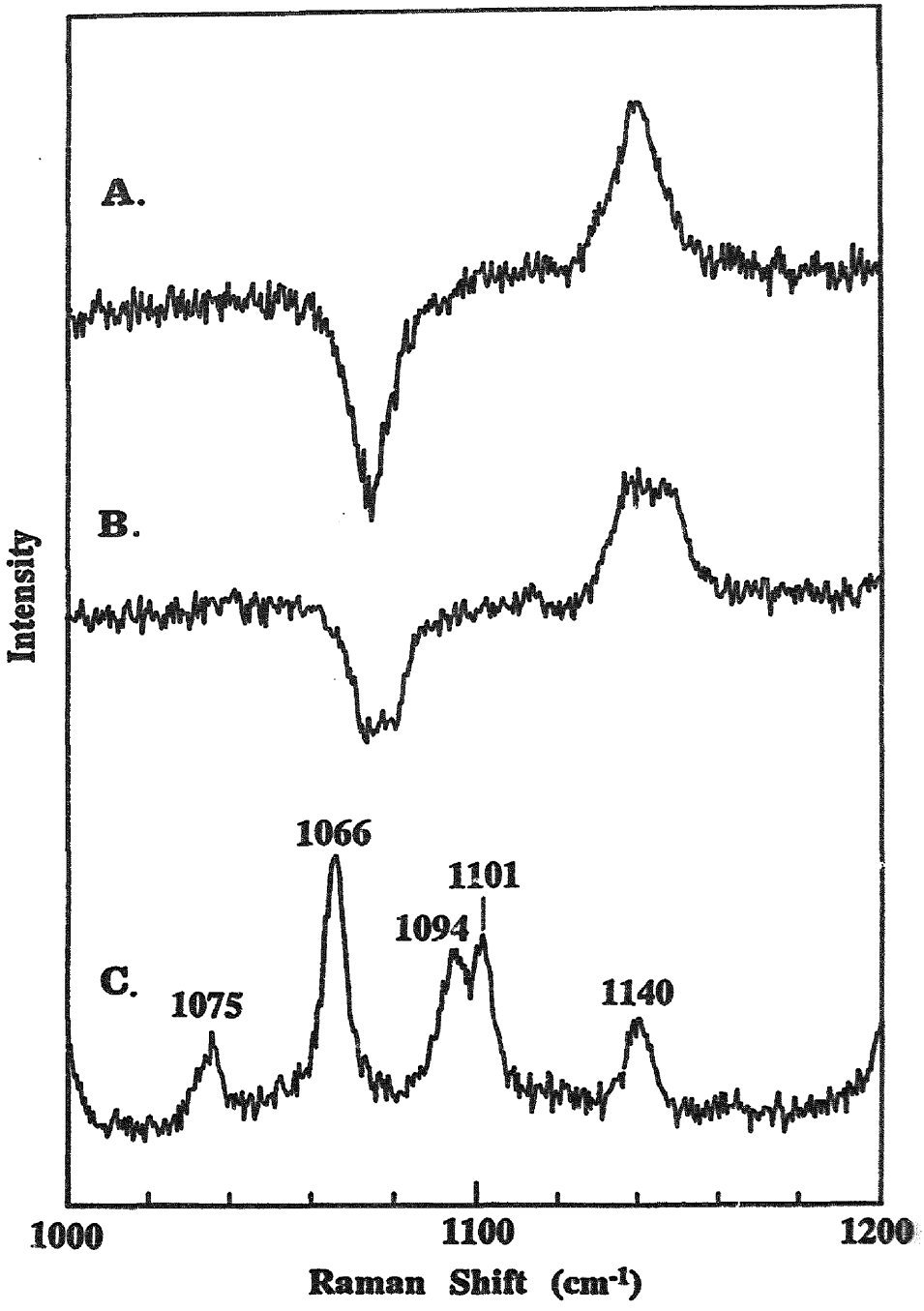
A.
B.
C.
Intensity
1066
1101
1094
1075
1140
1000
1100
1200
Raman Shift (cm-1)

4. Summary and conclusions

The complex spectral patterns observed in the RR spectra of dioxygen adducts of cobalt-substituted heme proteins and model compounds are shown to result from vibrational coupling of ν(O–O) with internal modes of the trans-axial ligand or intimately associated solvent or solute molecules. The conventional Fermi resonance equations, applied to data obtained for multiple isotopomers, can be employed to extract the actual inherent frequencies of the ν(O–O) and the coupled internal modes of the ligand, solute or substrate. Recent theoretical treatments validate the use of these equations for the interaction of two fundamental modes within different fragments of intermolecular complexes [88–91,105]. The excellent agreement between theory and experiment is illustrated in Fig. 14, as presented earlier in the paper.

While the existence of such complications underscore the need for high-quality spectra and cautious interpretation, the studies summarized here clearly demonstrate the potential utility of such vibrational coupling interactions. Thus, even quite subtle structural perturbations, which may not be sufficiently strong to produce shifts in the inherent frequency of the ν(O–O) mode, can be documented by the (sometimes quite remarkable) effects such structural changes produce in the observed resonance Raman spectral patterns.

Acknowledgements

The work conducted in the authors' laboratory which is summarized in this article was supported by grants from the National Institutes of Health (DK 35153 to J.R.K.) and the Polish State Committee for Scientific Research (2P 303 060 05 to L.M.P.). The authors thank Professor Jeanne McHale of the University of Idaho for providing a copy of her manuscript prior to its publication.

References

[1] W.S. Caughey (Ed.), Biochemical and Clinical Aspects of Oxygen, Academic Press, New York, 1979.
[2] E. Antonini, L. Rossi-Bernardi and E. Chiancone (Eds.), Methods in Enzymology; Hemoglobins, vol. 76, 1981.
[3] G. Fermi and M.F. Perutz, Haemoglobin and Myoglobin, D.C. Philips and F.M. Richards (Eds.), Atlas of Molecular Structures in Biology, Clarendon Press, Oxford, 1981, vol. 2.
[4] C. Ho (Ed.), Hemoglobin and Oxygen Binding, Elsevier Biomedical, New York, 1982.
[5] R.E. Dickerson and I. Geis, Hemoglobin: Structure, Function, Evolution and Pathology, The Benjamin/Cummings Publishing Co., Menlo Park, CA, 1983.
[6] M.F. Perutz, Mechanism of Cooperativity and Allosteric Regulation in Proteins, Cambridge University Press, Cambridge, 1990.
[7] S.E.V. Philips and B.P. Schoenborn, Nature (London), 292 (1981) 81.
[8] B. Shaanan, Nature (London), 296 (1982) 683.
[9] B. Shaanan, J. Mol. Biol., 171 (1983) 31.

[10] M.P. Mims, A.G. Porras, J.S. Olsen, R.W. Noble and J.A. Peterson, J. Biol. Chem., 258 (1983) 14219.
[11] H.C. Lee, M. Ikeda-Saito, T. Yonetani, R.S. Magliozo and J. Peisach, Biochemistry, 31 (1992) 7274.
[12] P. Jewsbury and T. Kitagawa, Biophys. J., 68 (1995) 1283.
[13] L.M. Miller amd M.R. Chance, Biochemistry, 34 (1995) 10170.
[14] S.E.V. Philips, J. Mol. Biol., 141 (1980) 531.
[15] M. Tsubaki and N.T. Yu, Proc. Natl. Acad. Sci. USA, 78 (1981) 3581.
[16] H.C. Mackin, M. Tsubaki and N.T. Yu, Biophys. J., 41 (1983) 349.
[17] W.T. Potter, M.P. Tucker, R.A. Houtchens and W.S. Caughey, Biochemistry, 26 (1987) 4699.
[18] L.M. Miller and M.R. Chance, J. Am. Chem. Soc., 116 (1994) 9662.
[19] L.M. Miller, M. Patel and M.R. Chance, ibid., 118 (1996) 4511.
[20] J.P. Collman, R.R. Gagne, T.R. Halbert, J.C. Marchon and C.A. Reed, ibid., 95 (1973) 7868.
[21] J.P. Collman, R.R. Gagne, C.A. Reed, T.R. Halbert, G. Lang and W.T. Robinson, ibid., 96 (1974) 1427.
[22] J.P. Collman, J.I. Brauman and K.S. Suslick, ibid., 97 (1975) 7185.
[23] J.P. Collman, J.I. Brauman, K.M. Doxsee, T.R. Halbert, E. Brunnenberg, R.E. Linder, G.N. LaMar, J. Del Gaudio, G. Lang and K. Spartalian, ibid., 102 (1980) 4182.
[24] J.P. Collman, J.I. Brauman, K.M. Doxsee, J.L. Sesler, R.M. Morris and Q.H. Gibson, Inorg. Chem., 22 (1983) 1427.
[25] J. Almog, J.E. Baldwin, R.L. Dryer and M. Peters, J. Am. Chem. Soc., 97 (1975) 226.
[26] J.P. Collman, J.I. Brauman, T.J. Collins, B.L. Iverson and J.L. Sessler, ibid., 103 (1981) 2450.
[27] J. Almog, J.E. Baldwin, M.J. Crossley, J.F. De Bernardis, R.L. Dryer, J.R. Huff and M. Peters, Tetrahedron, 37 (1981) 3589.
[28] M. Shimizu, F. Basolo, M.N. Vallejo and J.E. Baldwin, Inorg. Chim. Acta, 91 (1984) 247 and 251.
[29] J.E. Baldwin, J.H. Cameron, M.J. Crossley and E.J. Dayley, J. Chem. Soc., Dalton Trans., (1984) 1739.
[30] H. Dieckman, C.K. Chang and T.G. Traylor, J. Am. Chem. Soc., 93 (1971) 4086.
[31] H. Ogoshi, H. Sugimoto and Z. Yoshida, Tetrahedron Lett., (1976) 4481.
[32] J.E. Baldwin, M.J. Crossley, T. Klose, E.A. O'Rear III and M. Peters, Tetrahedron, 38 (1981) 21.
[33] T.P. Wijesekera, J.B. Paine III, D. Dolphin, F.W.P. Einstein and T. Jones, J. Am. Chem. Soc., 105 (1983) 6747.
[34] J. Mispelter, M. Momenteau, D. Lavalette and J.M. Lhotse, ibid., 105 (1983) 5165.
[35] T.G. Traylor, S. Tsuchiya, D. Campbell, M. Mitchell, D. Stynes and N. Koga, ibid., 107 (1985) 604.
[36] M. Momenteau, J. Mispelter, B. Loock and J.M. Lhotse, J. Chem. Soc., Perkin Trans., 1, (1985) 221.
[37] Y. Uemori, A. Nakatsubo, H. Imai, S. Nakagawa and E. Kyuno, Inorg. Chim. Acta, 124 (1985) 153.
[38] M. Momenteau, B. Loock, C. Tetreau, D. Lavalette, A. Croisy, C. Schaeffer, C. Huel and J. Lhotse, J. Chem. Soc., Perkin Trans., 2, (1987) 249.
[39] Y. Uemori, H. Miyakawa and E. Kyuno, Inorg. Chem., 27 (1988) 377.
[40] A. Desbois, M. Momenteau and M. Lutz, ibid., 28 (1989) 825.
[41] see for example: K. Nakamoto, Infrared and Raman Spectra of Inorganic and Coordination Compounds, A Wiley-Interscience Publication, J. Wiley and Sons, 4th edition, New York, 1986.
[42] F.S. Parker, Application of Infrared, Raman and Resonance Raman Spectroscopy in Biochemistry, Plenum Press, New York, 1983.
[43] T.G. Spiro (Ed.), Biological Application of Raman Spectroscopy, A Wiley-Interscience Publication, J. Wiley and Sons, New York, 1988, vol. 3.
[44] Methods in Enzymology, Academic Press, Inc., New York, 1993, vol. 226.
[45] Ibid., 1995, vol. 246.
[46] T.C. Strekas and T.G. Spiro, Biochim. Biophys. Acta, 263 (1972) 830.
[47] S. Asher, Methods Enzymol., 76 (1981) 371.
[48] J.M. Friedman, D.L. Rousseau and M.R. Ondrias, Ann. Rev. Phys. Chem., 33 (1982) 471.
[49] T.G. Spiro, Iron Porphyrins, A.P.B. Lever and H.B. Gray (Eds.), Addison-Wesley, Reading, MA, 1983, vol. 2. p. 89.
[50] W.A. Oertling, R.T. Kean, R. Wever and G.T. Babcock, Inorg. Chem., 29 (1990) 2633.

[51] S. Hirota, T. Ogura, E.H. Appelman, K. Shinzawa-Itoh, S. Yoshikawa and T. Kitagawa, J. Am. Chem. Soc., 116 (1994) 10564.
[52] S. Jeyarajah, L.M. Proniewicz, H. Bronder and J.R. Kincaid, J. Biol. Chem., 269 (1994) 31047.
[53] T. Kitagawa and Y. Mizutani, Coord. Chem. Rev., 135/136 (1994) 685.
[54] N.T. Yu, Methods Enzymol., 130 (1986) 350.
[55] B.M. Hoffman and D.H. Petering, Proc. Natl. Acad. Sci. USA, 67 (1970) 637.
[56] C.A. Spilburg, B.M. Hoffman and D.H. Petering, J. Biol. Chem., 247 (1972) 4219.
[57] T. Yonetani, H. Yamamoto and T. Iizuka, ibid., 249 (1974) 2168.
[58] R.S. Drago, T. Bengelsdijk, J.A. Breese and J.A. Connady, J. Am. Chem. Soc., 100 (1978) 5374.
[59] J.P. Collman, T.R. Halbert and K.S. Suslick, Metal Ions in Biology, T.G. Spiro (Ed.), A Wiley-Interscience Publication, J. Wiley and Sons, New York, 1980, vol. 2, ch. 1.
[60] K. Bajdor, J.R. Kincaid and K. Nakamoto, J. Am. Chem. Soc., 106 (1984) 7741.
[61] L.M. Proniewicz, A. Bruha, K. Nakamoto, Y. Uemori, E. Kyuno and J.R. Kincaid, ibid., 113 (1991) 9100.
[62] L.M. Proniewicz, J. Golus, H. Majcherczyk, K. Bajdor and J.R. Kincaid, J. Phys. Chem., 98 (1994) 12856.
[63] L.M. Sverdlov, M.A. Kovner and E.P. Krainov, Vibrational Spectra of Polyatomic Molecules, Halsted Press, New York, 1974, p. 522.
[64] D.P. DiLella and H.D. Stidham, J. Raman Spectrosc., 9 (1980) 90.
[65] D. Lin-Vien, N.B. Colthup, W.G. Fateley and J.G. Grasselli, The Handbook of Infrared and Raman Characteristic Frequencies of Organic Molecules, Academic Press, Inc., New York 1991.
[66] T. Watanabe, T. Ama and K. Nakamoto, J. Phys. Chem., 88 (1984) 440.
[67] A. Bruha and J.R. Kincaid, J. Am. Chem. Soc., 110 (1988) 6006.
[68] L.M. Proniewicz, K. Nakamoto and J.R. Kincaid, ibid., 110 (1988) 4541.
[69] C. Veas and J.L. McHale, ibid., 111 (1989) 7042.
[70] L.M. Proniewicz, J. Golus, K. Nakamoto and J.R. Kincaid, J. Raman Spectrosc., 26 (1995) 27.
[71] L.M. Proniewicz and J.R. Kincaid, J. Am. Chem. Soc., 112 (1990) 675.
[72] J.S. Valentine, R.P. Sheridan, L.C. Allen and P.C. Kahn, Proc. Natl. Acad. Sci. USA, 76 (1979) 1009.
[73] R. Quinn, J. Mercer-Smith, J.N. Burstyn and J.S. Valentine, J. Am. Chem. Soc., 106 (1984) 4136.
[74] P. O'Brien and D.A. Sweigart, Inorg. Chem., 24 (1985) 1405.
[75] T.G. Traylor and R. Popovitz-Biro, J. Am. Chem. Soc., 110 (1988) 239.
[76] K.A. Hagen, C.M. Schwab, J.O. Edwards, J.G. Jones, R.G. Lawler and D.A. Sweigart, ibid., 110 (1988) 7024.
[77] L.M. Proniewicz, A. Bruha, K. Nakamoto, E. Kyuno and J.R. Kincaid, ibid., 111 (1989) 7050.
[78] L.M. Proniewicz, Vib. Spectrosc., 2 (1991) 135.
[79] S. Salama and T.G. Spiro, J. Am. Chem. Soc., 100 (1978) 1105.
[80] M.A. Walters and T.G. Spiro, Inorg. Chem., 22 (1982) 4014.
[81] C.M. Jones, C.R. Johnson, S.A. Asher and R.E. Shepherd, J. Am. Chem. Soc., 107 (1988) 3772.
[82] C. Perchard and A. Novak, J. Chem. Phys., 48 (1968) 3079.
[83] S.M. Wang, L.Y. Lee and J.T. Chen, Spectrochim. Acta, 35A (1979) 765.
[84] J.R. Kincaid, L.M. Proniewicz, K. Bajdor, A. Bruha and K. Nakamoto, J. Am. Chem. Soc., 107 (1985) 6775.
[85] W.R. Scheidt and D.M. Chipman, ibid., 108 (1986) 1163.
[86] E. Fermi, Z. Phys., 71 (1931) 250.
[87] G. Herzberg, Molecular Spectra and Structure, Van Nostrand, New York, 1945, vol. 2, p. 215.
[88] M. Lax, J. Phys. Chem. Solids, 25 (1964) 487.
[89] C.H. Wang and J.L. McHale, J. Chem. Phys., 72 (1980) 4039.
[90] G. Irmer, V.V. Toporov, B.H. Bairamov and J. Monecke, J. Phys. Status Solidi B, 119 (1983) 595.
[91] J. Monecke, J. Raman Spectrosc., 18 (1987) 477.
[92] J. Odo, H. Imai, E. Kyuno and K. Nakamoto, J. Am. Chem. Soc., 110 (1988) 742.
[93] I. Ashikawa and K. Itoh, Biopolymers, 18 (1979) 1859.
[94] J.B. Hodgson, G.C. Percy and D.A. Thornton, J. Mol. Struct., 66 (1980) 75 and 81.

[95] T. Kitagawa, M.R. Ondrias, D.L. Rousseau, M. Ikeda-Saito and T. Yonetani, Nature (London), 298 (1982) 869.
[96] S. Hu, A.J. Schneider and J.R. Kincaid, J. Am. Chem. Soc., 113 (1991) 4815.
[97] P.R. Ortiz de Montellano (Ed.), Cytochrome P450. Structure, Mechanism, and Biochemistry, Plenum Press, New York and London, 1995.
[98] T.L. Poulos, B.C. Finzel and A.J. Howard, J. Mol. Biol., 195 (1987) 687.
[99] R. Raag and T.L. Poulos, Biochemistry, 28 (1989) 917.
[100] R. Raag, S.A. Martinis, S.G. Sligar and T.L. Poulos, ibid., 30 (1991) 11420.
[101] R. Raag, H. Li, B.C. Jones and T.L. Poulos, ibid., 32 (1993) 4571.
[102] M. Schappacher, L. Ricard, R. Weiss, R. Montiel-Montoya, E. Bill, U. Gonser and A. Trautwein, J. Am. Chem. Soc., 103 (1981) 7646.
[103] G. Chottard, M. Schappacher, L. Ricard and R. Weiss, Inorg. Chem., 23 (1984) 4557.
[104] O. Bangcharoenpaurpong, A.K. Rizos, P.M. Champion, D. Jollie and S. Sligar, J. Biol. Chem., 261 (1986) 8089.
[105] D.C. Daniel and J.L. McHale, J. Chem. Phys., submitted.